Hybrid Concrete for Advancing Pavement Performance

Final Report
October 2018

Sponsored by
Iowa Highway Research Board
(IHRB Project TR-708B)
Midwest Transportation Center
U.S. DOT Office of the Assistant Secretary
for Research and Technology

IOWA STATE UNIVERSITY
Institute for Transportation

About MTC

The Midwest Transportation Center (MTC) is a regional University Transportation Center (UTC) sponsored by the U.S. Department of Transportation Office of the Assistant Secretary for Research and Technology (USDOT/OST-R). The mission of the UTC program is to advance U.S. technology and expertise in the many disciplines comprising transportation through the mechanisms of education, research, and technology transfer at university-based centers of excellence. Iowa State University, through its Institute for Transportation (InTrans), is the MTC lead institution.

About InTrans

The mission of the Institute for Transportation (InTrans) at Iowa State University is to develop and implement innovative methods, materials, and technologies for improving transportation efficiency, safety, reliability, and sustainability while improving the learning environment of students, faculty, and staff in transportation-related fields.

ISU Non-Discrimination Statement

Iowa State University does not discriminate on the basis of race, color, age, ethnicity, religion, national origin, pregnancy, sexual orientation, gender identity, genetic information, sex, marital status, disability, or status as a U.S. veteran. Inquiries regarding non-discrimination policies may be directed to Office of Equal Opportunity, 3410 Beardshear Hall, 515 Morrill Road, Ames, Iowa 50011, Tel. 515-294-7612, Hotline: 515-294-1222, email eooffice@iastate.edu.

Notice

The contents of this report reflect the views of the authors, who are responsible for the facts and the accuracy of the information presented herein. The opinions, findings and conclusions expressed in this publication are those of the authors and not necessarily those of the sponsors.

This document is disseminated under the sponsorship of the U.S. DOT UTC program in the interest of information exchange. The U.S. Government assumes no liability for the use of the information contained in this document. This report does not constitute a standard, specification, or regulation.

The U.S. Government does not endorse products or manufacturers. If trademarks or manufacturers' names appear in this report, it is only because they are considered essential to the objective of the document.

Quality Assurance Statement

The Federal Highway Administration (FHWA) provides high-quality information to serve Government, industry, and the public in a manner that promotes public understanding. Standards and policies are used to ensure and maximize the quality, objectivity, utility, and integrity of its information. The FHWA periodically reviews quality issues and adjusts its programs and processes to ensure continuous quality improvement.

Iowa DOT Statements

Federal and state laws prohibit employment and/or public accommodation discrimination on the basis of age, color, creed, disability, gender identity, national origin, pregnancy, race, religion, sex, sexual orientation or veteran's status. If you believe you have been discriminated against, please contact the Iowa Civil Rights Commission at 800-457-4416 or the Iowa Department of Transportation affirmative action officer. If you need accommodations because of a disability to access the Iowa Department of Transportation's services, contact the agency's affirmative action officer at 800-262-0003.

Technical Report Documentation Page

1. Report No. IHRB Project TR-708B	**2. Government Accession No.**	**3. Recipient's Catalog No.**	
4. Title and Subtitle Hybrid Concrete for Advancing Pavement Performance		**5. Report Date** October 2018 **6. Performing Organization Code**	
7. Author(s) Kejin Wang (orcid.org/0000-0002-7466-3451) and Jinxiang Hong (orcid.org/0000-0002-7466-3451)		**8. Performing Organization Report No.**	
9. Performing Organization Name and Address Civil, Construction, and Environmental Engineering Iowa State University 394 Town Engineering Ames, IA 50011		**10. Work Unit No. (TRAIS)** **11. Contract or Grant No.** Part of DTRT13-G-UTC37	
12. Sponsoring Organization Name and Address Midwest Transportation Center 2711 S. Loop Drive, Suite 4700 Ames, IA 50010-8664 Iowa Highway Research Board Iowa Department of Transportation 800 Lincoln Way Ames, IA 50010	U.S. Department of Transportation Office of the Assistant Secretary for Research and Technology 1200 New Jersey Avenue, SE Washington, DC 20590	**13. Type of Report and Period Covered** Final Report **14. Sponsoring Agency Code**	
15. Supplementary Notes Visit www.intrans.iastate.edu for color pdfs of this and other research reports.			

16. Abstract

Rutting, caused by a depression or groove of traveling wheels worn into a road, is a major problem of conventional asphalt or flexible pavements, and is primarily due to plastic deformation of the asphalt concrete near the pavement surface. To overcome this problem, a hybrid, made with asphalt (flexible) pervious concrete filled with Portland cement (rigid) mortar, called casting cement asphalt mixture (CCAM), has been developed.

During the development process, various CCAMs were made with Iowa concrete materials. Experiments were conducted to gauge optimal porosity of asphalt pervious concrete and optimal flowability of mortar for CCAMs. The basic engineering properties of these CCAMs, such as strength, shrinkage, and freeze-thaw durability, were evaluated.

The results show that CCAMs can be produced successfully by using pervious concrete of 25% porosity and rapid set cement grout with very high flowability. The calcium sulphoaluminate cement grout used in this study attained strength greater than 18 MPa (2,600 psi) in less than 12 hours. Therefore, a CCAM pavement could open to traffic at a much earlier time than a conventional Portland cement concrete roadway. While asphalt concrete displayed a 9 mm rut after being subjected to 10,000 wheel track cycles during a wheel track rutting test, the CCAM showed a less than 1 mm rut. However, as the CCAM is neither asphalt nor Portland cement concrete, a big project challenge was to find appropriate test methods for evaluating key properties of CCAM, especially the method for testing its freeze-thaw durability.

Although CCAM has attracted a great deal of attention in Europe and Asia, most applications have been in warm climate regions. Few applications of CCAM have been conducted in the US, especially in cold climate regions. Further investigation needs to be done on the CCAM freeze-thaw durability before this new material is applied to Iowa pavements.

17. Key Words CCAM—freeze-thaw—pervious concrete—self-consolidating grout/mortar—semi-flexible concrete—shrinkage		**18. Distribution Statement** No restrictions.	
19. Security Classification (of this report) Unclassified.	**20. Security Classification (of this page)** Unclassified.	**21. No. of Pages** 74	**22. Price** NA

Form DOT F 1700.7 (8-72) **Reproduction of completed page authorized**

HYBRID CONCRETE FOR ADVANCING PAVEMENT PERFORMANCE

Final Report
October 2018

Principal Investigator
Kejin Wang, Professor
Civil, Construction, and Environmental Engineering, Iowa State University

Principal Collaborator
Jinxiang Hong, Senior Researcher
Jiangsu Research Institute of Building Science, Subote New Materials Co., Ltd.

Authors
Kejin Wang and Jinxiang Hong

Sponsored by
Midwest Transportation Center,
U.S. Department of Transportation
Office of the Assistant Secretary for Research and Technology,
and Iowa Highway Research Board
(IHRB Project TR-708B)

Preparation of this report was financed in part
through funds provided by the Iowa Department of Transportation
through its Research Management Agreement with the
Institute for Transportation

A report from
Institute for Transportation
Iowa State University
2711 South Loop Drive, Suite 4700
Ames, IA 50010-8664
Phone: 515-294-8103 / Fax: 515-294-0467
www.intrans.iastate.edu

TABLE OF CONTENTS

LIST OF FIGURES

LIST OF TABLES

LIST OF ABBREVIATIONS

Asphalt concrete (AC)

Air-entraining agent (AEA)

Casting cement asphalt mixture (CCAM)

Cement-based grout (CSG)

Dynamic stability (DS)

Electron dispersive spectroscopy (EDS)

Early-strength grout (ESG)

Fly ash (FA)

Grouting material (GM)

High modulus asphalt concrete (HMAC)

High-range water-reducing admixture (HWRA)

High-strength grout (HSG)

Indirect tensile strength (IDT)

Portland cement (PC)

Porous asphalt mixture (PAM)

Self-consolidating concrete (SCC)

Silica fume (SF)

Shrinkage-reducing admixture (SRA)

Voids in coarse aggregate on the dry rodded condition (VCA_{DRC})

Voids in coarse aggregate of the compacted mixture (VCAmix)

ACKNOWLEDGMENTS

The authors would like to acknowledge the Midwest Transportation Center, the U.S. Department of Transportation Office of the Assistant Secretary for Research and Technology, the Iowa Highway Research Board, and the Iowa Department of Transportation for sponsoring this research. This was one of four pilot projects for novel or innovative ideas and fundamental advances that were sponsored.

Special support for the project from the Institute for Transportation and the Department of Civil, Construction, and Environmental Engineering at Iowa State University is also greatly appreciated.

Visiting Scholar Jinxiang Hong from Jiangsu Research Institute of Building Science, Jiangsu, China, led the experimental work through the entire project during his one-year stay at ISU. Graduate student Paul Ledtje helped greatly on the testing of pervious asphalt concrete and Yifeng Ling helped on some grout hybrid concrete tests. Undergraduate student Mingsui Tang was involved in the freeze-thaw and shrinkage tests. Visiting Professor Chuanqing Fu assisted in the preparation of the mixtures for the research. Laboratory Manager Bob Steffes assisted in much of the detailed work conducted in Iowa State's Portland Cement Concrete Research Laboratory. The project would not have been completed successfully without the contributions of the above-mentioned individuals.

EXECUTIVE SUMMARY

Goals and Objectives

The goals of this project were to explore the advantages, challenges, and feasibility of using a hybrid, semi-flexible, semi-rigid concrete for highway pavements, bridge decks, and overlays. Specifically, the objectives were as follows:

- Develop a hybrid concrete, a casting cement asphalt mixture (CCAM), using raw materials sourced locally in Iowa
- Evaluate key engineering properties, including rutting, shrinking, and freeze-thaw resistance, for the hybrid concrete in Iowa's environment and for its transportation needs
- Provide insights and recommendations to develop guidelines for applying the CCAM in practice

Problem Statement

Although this hybrid concrete has been adopted in warmer climates in Europe and Asia, its uses in the US have not been well understood or studied.

Background

CCAMs were first designed in the 1950s to protect the surface course from oils and fuels. It has been used since that time throughout Europe and Asia, and the asphalt mixture has performed well in withstanding stress induced from heavy traffic loads and sudden braking. In particular, research has demonstrated that CCAMs can significantly improve rutting resistance on flexible pavements.

While the asphalt mixture has worked well on pavements in warmer climates, methods utilizing grouting materials are currently being developed to improve its low-temperature performance and moisture susceptibility.

Project Description

To develop a CCAM using Iowa materials, the research team performed the following tasks:

1. Collected and characterized the general properties of local coarse and fine aggregates, asphalt, cement, and admixtures
2. Designed an asphalt pervious concrete with porosity levels of 25 percent, and examined its basic properties, such as density, air void, draindown, and Cantabro abrasion
3. Designed a highly flowable Portland cement grout with high stability based on the concept of self-consolidating concrete, and tested its fluidity and strength

4. Achieved the optimal mix proportions for a porous asphalt mixture and cement-based grout using the local Iowa raw materials

Furthermore, the research team evaluated the key engineering properties and microstructure of the CCAM, which included conducting tests on compressive strength, shrinkage behaviors, and freeze-thaw durability.

Key Findings

- CCAMs can be successfully produced with a pervious concrete of 25 percent porosity and a highly flowable, rapid set cement grout
- The CCAM is strengthened with the addition of grouting material, particularly calcium sulphoaluminate cement grouting, as well as by utilizing a combination of fly ash and silica fume
- A high modulus grouting material can make a CCAM less susceptible to rutting

Implementation Readiness and Benefits

The hybrid concrete mixture has potential benefits not seen in traditional counterparts, including opening to traffic sooner than on a conventional cement concrete pavement, and a longer service life, a higher resilient modulus, and better rutting performance than traditional asphalt mixtures. This hybrid concrete uses Iowa materials and shows promising signs of reducing rutting in wheel paths, among other benefits.

While the research team successfully developed a CCAM that is designed for use on Iowa roadways and other cooler climate environments, further study is needed on its key properties, particularly freeze-thaw durability, before it can be applied to Iowa pavements.

Recommendations for Future Research

Because the CCAM was newly developed for Iowa roadways, more research is needed to understand its properties, particularly its freeze-thaw durability. The research team used ASTM C666-B for this test, but new test methods (such as testing slab sections in field environments) may be needed.

The grouting materials used contained a large portion of fine particles, which made proper air entrainment and a stable air system in the grout pastes very challenging. As a part of the freeze-thaw durability study, development of another technology to introduce a proper air system in the grout of the CCAM is also necessary.

Further research is also needed to prevent segregation and water bleeding, which in turn could adversely affect the formation of the microstructure and compressive strength due to overuse of superplasticizer to improve flowability.

INTRODUCTION

Background

Rutting, caused by a depression or groove of traveling wheels worn into a road, is a major problem of conventional asphalt or flexible pavements. Severe ruts can impede steering and significantly affect driving safety and comfort. Rutting often results from one or more of the following causes:

- Plastic deformation of the asphalt concrete near the pavement surface
- Continued compaction of the asphalt concrete under the action of traffic surface wear
- Wearing of the surface particles of the asphalt concrete by traffic (Ballestero et al. 2014)

In the case of plastic deformation, the asphalt concrete mix lacks the internal strength to resist permanent deformation under the stress imposed by vehicle tires. The internal strength is closely related to the friction characteristics of the concrete aggregates as well as the viscoelastic properties of the asphalt binder, which often becomes sufficiently viscous at an elevated pavement temperature and allows the pavement to deform under constant or slowly moving loads (Wu et al. 2010). To overcome this problem, a semi-flexible, semi-rigid pavement concrete, a hybrid between asphalt and Portland cement concretes, has been developed (Cai et al. 2017).

The semi-flexible, semi-rigid pavement concrete is made with asphalt pervious concrete filled with highly flowable Portland cement mortar in its large-sized voids. Since a Portland cement mortar is cast into asphalt pervious concrete, this resulting composite material is also called a casting cement asphalt mixture (CCAM) (Ding et al. 2012, Deng et al. 2016) (Figure 1.1).

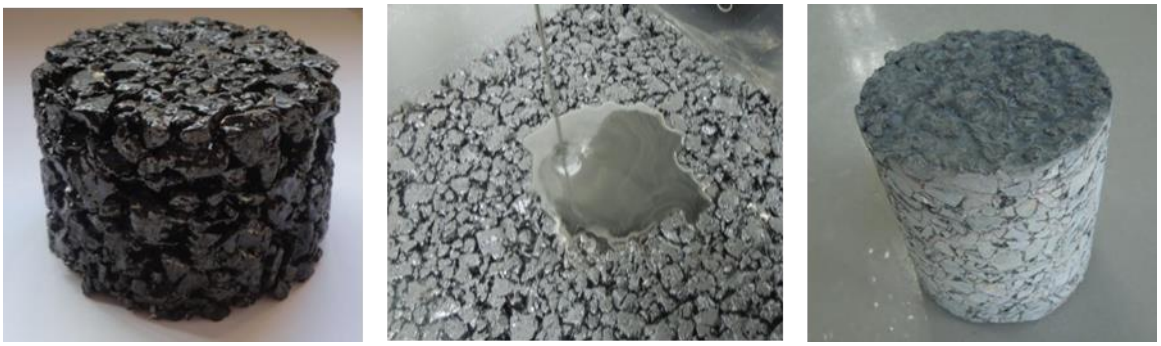

(a) Asphalt pervious concrete (b) Pouring cement mortar (c) CCAM cylinder sample

Figure 1.1. Casting cement asphalt mixture (CCAM)

Research has demonstrated that a CCAM can significantly improve rutting resistance of flexible pavements (Figure 1.2).

(a) Rutting in asphalt concrete (b) Little/no rutting in CCAM

Figure 1.2. Results from rutting tests of different pavement concrete

In addition, use of CCAMs for pavements will not require jointing as conventional rigid Portland cement concrete pavements do, since the framework of CCAM pavements is made with asphalt pervious concrete and is flexible (Mayer and Thau 2001).

CCAMs first originated in France in the 1950s. A CCAM was designed to protect the surface course from oils and fuels. A practical example of a CCAM application occurred at the Copenhagen Airport when more than 160,000 m^2 of the CCAM was applied (Koting et al. 2007) (see Figure 1.3).

Unknown image source

Figure 1.3. Application of CCAM at a European airport

Application of CCAMs also occurred in the airport and ports in Germany and the Netherlands. In recent years, CCAMs have gained greater acceptance due to their advantages. The principles and applications of CCAMs have gained recognition in many European countries as well. CCAMs were also introduced on public roads in Malaysia to address the rutting in heavy traffic areas, such as bus lanes, bus and car terminals, heavy traffic roads, etc. These joint-free, high-friction pavements perform superbly in withstanding the stress induced from heavy traffic loads and sudden braking (Setyawan 2006, Afonso et al. 2016).

The pavement performance of CCAMs and asphalt concrete have been compared in the literature. Methods to improve the low-temperature performance and moisture susceptibility of CCAMs were proposed by some researchers (Hao et al. 2003). To balance the flexible and rigid characteristics of the CCAM, the grouting materials were modified with superplasticizer and SBR LATEX (Fang et al. 2016). It was found that the CCAM exhibits better pavement performance than traditional asphalt mixtures except at low temperatures (Hou et al. 2016). A cyclic wheel load test for runway design was also introduced to determine the damage patterns in a CCAM (Yang and Weng 2015). A property-component relationship was established to investigate the connections between a CCAM's resilient modulus and its constitutional and volumetric characteristics (Wu et al. 2010). The influences of grouting materials and the asphalt matrix on a CCAM's properties were also studied by looking into the mechanical features (Setyawan 2013, Zhang et al. 2016, Pei et al. 2016).

CCAMs are now widely used in Japan and increasingly used in China (Ding et al. 2012, Deng et al. 2016). More than 50,000 square meters of Subote anti-rutting, semi-flexible pavement have been used in Nanjing, Yancheng, Suzhou, Changzhou, Wuhan, and other places.

The Nanjing Jiangning Chengxin Avenue intersection, for instance, required maintenance each year when ordinary asphalt pavement was used. Since 2012, Subote semi-flexible pavement anti-rutting technology has been applied there, and no rut has been observed so far (Figure 1.4).

Figure 1.4. Application of CCAM in Nanjing

Simultaneous comparison of rutting resistance effects was conducted between the semi-flexible pavement and the normal asphalt pavement applied on Yancheng provincial highway S231 and X303 intersection, respectively. After one year of operation, the rutting depth of the asphalt pavement had reached 5 cm, whereas the semi-flexible pavement had almost no rut. Usually, after one month of repair during the summer, the rut depth of the intersection of Yancheng G228 highway and S331 was 10 cm, requiring 3 to 4 annual maintenance repairs. However, since the Subote semi-flexible pavement treatment was applied in the intersection, good performance has been observed (Figure 1.5).

(a) Asphalt pavement

(b) CCAM pavement

Figure 1.5. Application of CCAM in Yancheng

A 5,000 square meter demonstration project was carried out in the construction of new BRT lanes in the Wuhan and Changzhou BRT maintenance program (Figure 1.6).

(a) Wuhan

(b) Changzhou

Figure 1.6. Application of CCAM in Wuhan and Changzhou Cities

The semi-flexible anti-rutting pavement cost was about 1.5 to 2 times that of ordinary asphalt pavement. Although the initial investment was a little higher, the service life was 10 times longer than for the ordinary asphalt pavement. This could significantly reduce annual maintenance time and costs and traffic congestion, as well as yield remarkable economic and social benefits.

To date, very little study of CCAMs has been conducted in the US. The synergistic effects of asphalt and Portland cement concrete on CCAMs are not well documented. Although the improvement in rutting resistance is evident, little is known about the mechanical behavior, shrinkage, stability, moisture susceptibility, freeze-thaw performance, and cracking resistance of CCAMs.

Objectives

The goals of this project were to explore the advantages, challenges, and feasibility of using a hybrid, semi-flexible, semi-rigid concrete for highway pavements, bridge decks, and overlays. The specific objectives were as follows:

- Develop the hybrid concrete using Iowa's local raw materials
- Evaluate the key engineering properties of hybrid concrete for Iowa environment and transportation needs (rutting, shrinkage, and freeze-thaw [F-T] resistance)
- Provide fundamental insights and recommendations to lead to development of guidelines for applying CCAMs in practice

Scope

The study was divided into three steps as follows:

The first step, presented in Chapters 2 and 3, was to develop a CCAM using Iowa materials. During this step, all raw materials commonly used in Iowa, such as coarse and fine aggregates, asphalt, cement, and admixtures, were collected and characterized for their general properties. Asphalt pervious concrete with porosity levels of 25% was designed and its basic properties, such as density, air void, draindown and Cantabro abrasion, were examined. A highly flowable Portland cement grout with high stability was designed using the concept of self-consolidating concrete (SCC) (ACI-Committee 2007), and its fluidity and strength were tested. Based on these test results, the optimal mix proportions of porous asphalt mixture and cement based grout with Iowa local raw materials were achieved.

The second step, presented in Chapter 4, was to evaluate the key engineering properties and microstructure of a CCAM. During this part of the project, the mechanical properties, such as compressive strength, indirect tensile strength, and elastic modulus were tested, and the shrinkage behaviors of a CCAM, including free dry shrinkage and autogenous shrinkage, were assessed. The freeze-thaw durability of the CCAM was also investigated. Finally, the microstructure of the CCAM, such as interfacial transition zones, hydrated products, and internal defects, was examined.

The third step, the conclusions and recommendations of this research, appear in Chapter 5. A summary of test data from the experiments conducted in this study was provided. A comparison of the present test data with corresponding data on asphalt and Portland cement concrete, the latter of which was collected from published literature, was carried out. This final project report was developed.

EXPERIMENT RAW MATERIALS

The types and sources of experimental raw materials used in this study are presented in Table 2.1.

Table 2.1. Raw materials and their sources

Materials		Type	Provider
Asphalt binder		PG76-28	Jebro Inc.
	Cement-based grout (CSG)	JGM201	China
Cementitious materials	Portland cement (PC)	Type I/II	Ash Grove
	Class C Fly ash (FA)	Class F	Headwater Resources
	Silica fume (SF)		
Admixtures	High-range water-reducing admixture (HWRA)	ADVA Cast 600	W. R. Grace
	Shrinkage-reducing admixture (SRA)	ECLIPSE 4500	W. R. Grace
	Air-entraining agent (AEA)	MasterAir VR10	BASF
Aggregates	Coarse aggregate	Limestone	Ft. Dodge Mine
	Fine aggregate	Limestone	Ft. Dodge Mine
	Mineral powder	Limestone	Ft. Dodge Mine

Asphalt Binder

The type PG76-28 asphalt binder used in this study is polymer modified. Its basic properties are shown in Table 2.2 and the traditional temperature-viscosity relationship is shown in Figure 2.1. Under Iowa climate conditions, this may result in unnecessarily high mixing and compaction temperatures, and the provider has suggested a mixing temperature range of 305 to 325°F, and compaction temperature range of 275 to 300°F.

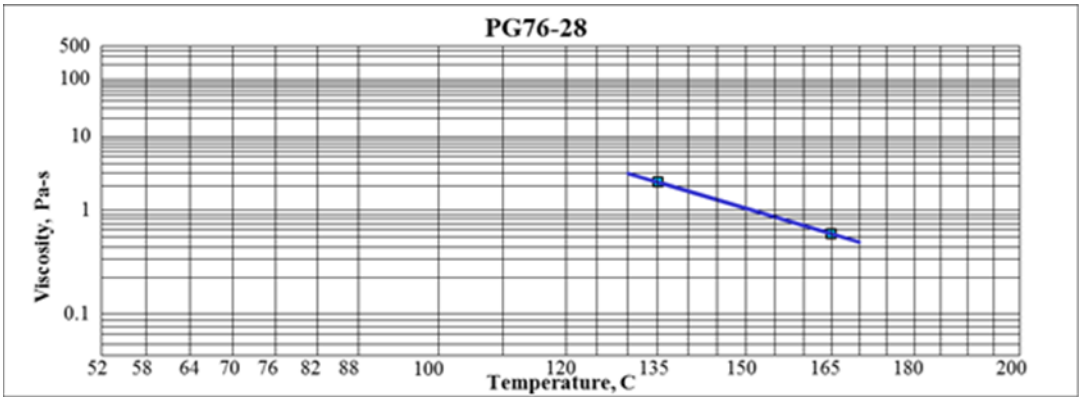

Figure 2.1. Temperature – viscosity relationship (provided by the supplier)

Table 2.2. Asphalt binder properties (provided by the supplier)

Parameter	Test method	Specification requirement	Result
Flash point, °C	T-48	>230	>230
Rotational Viscosity(@135°C), Pa.s	T-316	⩽3.0	2.100
Rotational Viscosity(@165°C), Pa.s	T-316	/	0.467
Original DSR(@76°C), kPa	T-315	⩾1.00	1.680
Phase Angle, °	T-315	/	60.10
RTFO DSR(@76°C), kPa	T-315	⩾2.20	3.470
BBR Creep Stiffness(@-18°C), MPa	T-313	⩽300	199
BBR "M" Value (@-18°C), s	T-313	⩾0.300	0.318
RTFO Mass Loss, %	T-240	⩽1.00	0.290
WYDOT ER(@25°C),%	T-301	⩾60%	92.50

Cementitious Materials

Two types of cement-based grout materials were used in this study. One was an early-strength grout (ESG), a packed product from China, and the other was developed using raw materials from Iowa.

Early-Strength Cement-Based Grout Materials

ESG, consisting of calcium sulphoaluminate cement, fine aggregate, filler, and various admixtures, is a medium-class strength grouting material used widely in China. It was used as a comparison sample in this study. The recommended amount of water for 100 kg of ESG is 30 to 32 liters and 31 liters were used. Table 2.3 shows the fluidity and setting time of ESG, and Figure 2.2 shows the strength development of ESG.

Table 2.3. Fluidity and setting time of ESG

	Fluidity(s)		Setting time (h:min)	
Test items	0 min	30 min	initial	final
Test result	15	18	2:00	2:30

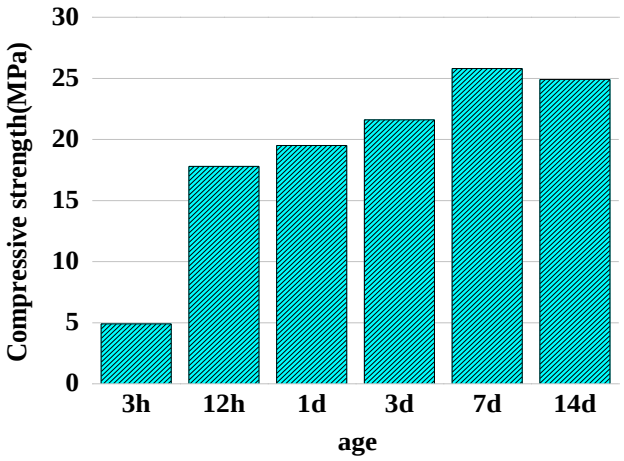

(a) Strength development of ESG

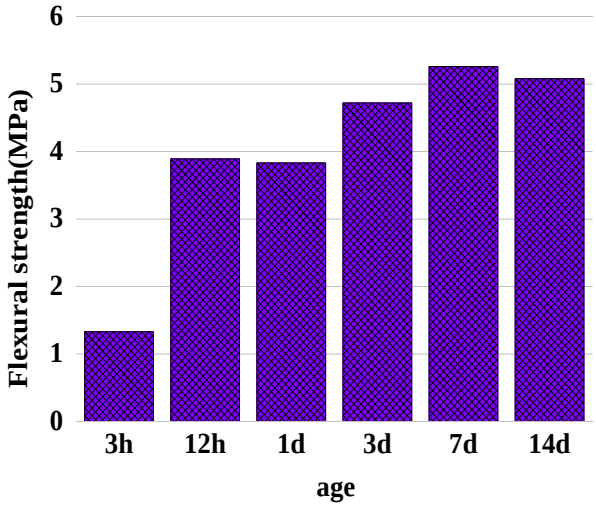

(b) Strength development of ESG

Figure 2.2. Strength development of ESG (1 MPa = 145 psi)

Portland Cement and SCMs

In order to develop the CCAM with Iowa local raw materials, Portland cement, fly ash, and silica fume were used to formulate a grout material. Type I/II Cement produced by Ash Grove Inc., the most widely used cement for many kinds of concrete construction in the West and Midwest, met the specification requirements for both ASTM C150 Type I and Type II. The physical and chemical properties are listed in Table 2.4

Table . The fly ash met the requirements of Class F.

Table 2.4. Physical and chemical properties of cementitious materials

Composition %	PC	FA
Na_2O	0.30	0.61
MgO	3.10	2.70
Al_2O_3	8.90	18.80
SiO_2	29.30	55.02
SO_3	3.10	0.40
K_2O	0.70	1.10
CaO	48.30	12.38
Fe_2O_3	4.10	5.62
LOI	1.70	1.18
Specific gravity	3.14	/
Fineness (m^2/kg)	490	/

Aggregates and Mineral Powder

Aggregates including coarse aggregate (≥4.75 mm), fine aggregate (≤2.36 mm), and mineral powder were used to prepare the porous asphalt mixture in this study. The coarse aggregate used was 1/2 in. crushed limestone, and the fine aggregate used was #4 river sand. Both coarse and fine aggregates were used in oven-dried condition. Properties of the aggregates and mineral powder are listed in Table 2.5.

Table 2.5. Properties of aggregates and mineral powder

Aggregate size	Coarse aggregate	Fine aggregate	Mineral powder
Apparent specific gravity (g/cm^3)	2.692	2.557	2.40
Bulk specific gravity (g/cm^3)	2.737	4.401	2.38
Uncompacted voids in the mineral, %	/	31	/
Water absorption (%)	0.98	4.167	/
Flat and elongated particles (%)	0	/	/
Flat and elongated particles (%) >9.5 mm	0	/	/
Flat and elongated particles (%) <9.5 mm	0	/	/
Crushed stone with one face (%)	100	/	/
Crushed stone with two or more faces (%)	100	/	/
G_{CA}, Specific gravity (g/cm^3)	2.670	/	/
Bulk density (g/cm^3)	1.591	/	/
VCA_{DRC} (%)	40.3	/	/

Coarse Aggregate (≥4.75 mm)

Selection of Coarse Aggregate—Coarse aggregate should have abrasion values of less than 30% in accordance with ASTM Test Method C131. Crushed gravel (if used) must have at least 90%

particles with two faces and 95% particles with one face resulting from crushing in accordance with ASTM Test Method D5821. The percentage of flat and elongated particles should not exceed 10%, with a ratio of 5:1 in maximum to minimum dimension, respectively, in accordance with ASTM Test Method D4791.

Fine Aggregate (≤2.36 mm)

Selection of Fine Aggregate—The fine aggregate should have an uncompacted voids content of least 40% when tested in accordance with ASTM Test Method C1252, Method C. It is important that the aggregate be clean. The sand equivalent value of the fine aggregate passing the 2.36 mm (No. 8) sieve, according to ASTM Test Method D2419, should be at least 45% or greater. It is recommended that the material to be tested be separated on the 2.36 mm (No. 8) sieve because of the coarse grading of the aggregate. It is also very important to remove any coatings or fines adhering to the coarse material.

Admixtures

Three admixtures, a high-range water-reducing admixture (HWRA), an air-entraining agent (AEA), and a shrinkage-reducing admixture (SRA), were used to prepare for high performance grout materials in this study. HWRA is a polycarboxylate-based, high-range water reducer designed for the production of self-consolidating concrete (SCC). It helps grout material obtain a very high flowability at a low level ratio of water to binder. SRA is a liquid admixture for concrete or mortar that can reduce drying shrinkage. Rather than functioning as an expansive agent, a SRA acts by reducing the surface tension of pore water. An AEA is a liquid neutralized vinsol resin product that provides freeze-thaw resistance, and also meets the requirements of ASTM C260, AASHTO M 154, and CRD-C13. Because of the severe cold climate conditions in Iowa, an AEA and a SRA are used to improve the freeze-thaw durability and cracking resistance of grout, and thus to improve the durability of the CCAM.

The dosage of HWRA was determined based on the trial mix, while the dosages of the SRA and the AEA were determined based on the recommendations provided by the manufacturers. Table 2.6 gives the dosages of chemical admixtures used in this project.

Table 2.6. Dosage of chemical admixtures

	Dosage, ml/kg*	
Admixture	**Recommended dosage**	**Actual dosage**
HWRA	1.3 ~ 6.5	12.0
SRA	0.4 ~ 4.0	3.0
AEA	0.16 ~ 2.6	1.0

* Total weight of cementitious materials

MIX PROPORTION DESIGN

Design Requirement

Design requirements of pervious concrete are listed in Table 3.1**Error! Reference source not found.**. The air voids are required to be approximately 25%. Draindown amount of pervious concrete is limited to below 0.3%.

Table 3.1. Design requirement of pervious concrete

Test items	Technology requirement
Air void (%)	25±2
Draindown （%）	⩽0.3
Cantabro abrasion (%)	/

Property requirements of cement are given in Table 3.2**Error! Reference source not found.**. The fluidities of cement tested at 0 and 30 min are both required to be around 20±4 s. The compressive strength should be no less than 20 MPa.

Table 3.2. Property requirements of cement

Test items		Technology requirement
Fluidity(s)	0 min	20±4
	30 min	20±4
Compressive strength (MPa)		≥20

Mix Proportion Design of Porous Asphalt Mixture (PAM)

Procedure for Mixing and Compacting

Porous asphalt mixture was fabricated at the National Concrete Pavement Technology Center Laboratory at Iowa State University. Asphalt binder, together with aggregates and mineral powder, were mixed in a bowl shown in Figure 3.1. Afterwards, loose asphalt mixture was compacted by using a gyratory compactor, as displayed in Figure 3.2.

Figure 3.1. Mixer of asphalt mixture

Figure 3.2. Gyration compaction meter

As illustrated in Table 3.3, aggregate, together with mineral powder, was heated to 385–405°F while asphalt was heated to 305–325°F. The compacting temperature was set to be around 275–300°F.

Table 3.3. Temperature control during mixing and compaction

Raw materials	Temperature/°F (°C)
Aggregate and Mineral powder	385–405°F (175°C)
Asphalt	305–325°F (175°C)
Compacting temperature	275–300°F (170°C)

Aggregates were first mixed with asphalt binder for 45 s. Then mineral powder was blended in, and the mixture was mixed for 90–150 s. The entire mixture was cured in an oven for 2 hours at 275–300°F to simulate the short-term aging of asphalt mixture during transportation and the compaction process in the field. The compaction parameter is given in Table 3.4. As shown in Figure 3.3, the number of gyrations is determined as 50 according to the density-gyration curve.

Table 3.4. Compaction parameter

Consolidation pressure	600 kPa
Angle of gyration	1.16° internal, 1.25° external
Speed of gyration	30 r /min
Number of gyrations	50 gyrations

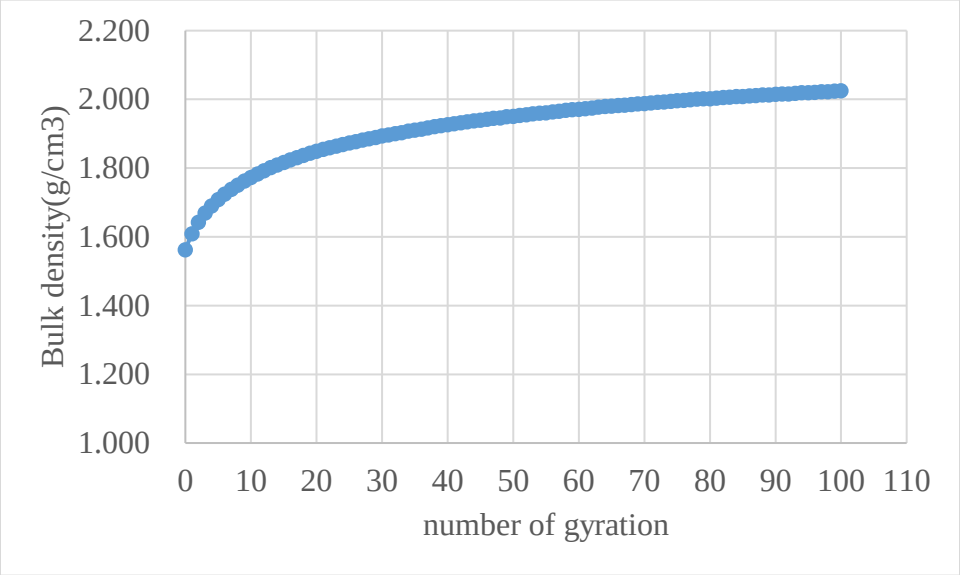

Figure 3.3. Density-gyration curve

Aggregate Gradation Design

Limestone coarse aggregate and river sand were sieved. According to the sieving results, the mass percentages of aggregates, mineral powder, and asphalt were calculated and appear in Table 3.5. The gradation curves of coarse and fine aggregates are shown in Table 3.6 and Figure 3.4. Both coarse and fine aggregates gradations are located within the ASTM specification band, which indicates they are properly graded.

Table 3.5. Mass percentage of different components in asphalt mixture

Raw materials	Type (mm[in.])	Weight (%)
Aggregate	12.5(1/2 in.) ~ 19 mm (3/4 in.)	13.6
	9.5 (3/8 in.) ~ 12.5 mm (1/2 in.)	38.8
	4.75 (No. 4) ~ 9.5 mm (3/8in.)	35.0
	<2.36 mm (No. 8)	7.8
Mineral powder	<0.075 mm (No. 200)	1.9
Asphalt	PG 76–28	2.9

Table 3.6. Blend gradation of aggregate

	Percent passing by mass (%)	
Sieve size	Specification requirement	Test result
3/4 in. (19.0 mm)	100	100.0
1/2 in. (12.5 mm)	85–100, 80–95	86.2
3/8 in. (9.5 mm)	35–60, 14–65	48.2
No. 4 (4.75 mm)	10–25, 5–25	10.8
No. 8 (2.36 mm)	5–10, 5–15	10.0
No. 16 (1.18 mm)	/,4–10	6.5
No. 30 (0.6 mm)	/,3–8	5.2
No. 50 (0.3 mm)	/,2–6	4.5
No. 100 (0.15 mm)	/,2–5	4.0
No. 200 (0.075 mm)	2–4, 1–4	3.7

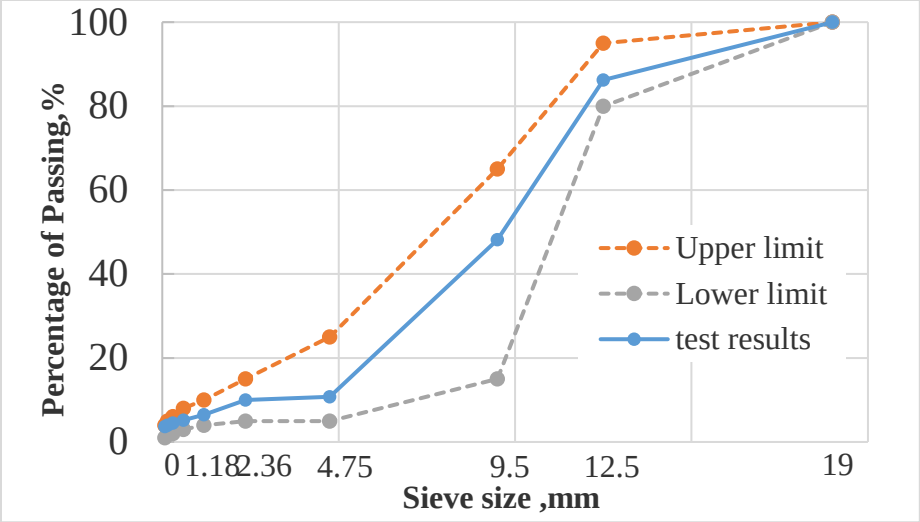

Figure 3.4. Gradation of porous asphalt mixture

Selection of Optimum Asphalt Content

Due to the time limitation, the asphalt content of porous asphalt concrete was set as 2.9% in this project, according to the practical experience in China. Subsequent test results of this asphalt mixture all meet the specification requirements, which indicates that the selection of optimum asphalt content was reasonable.

Volumetric Properties of Porous Asphalt Mixture

The theoretical maximum specific gravity, theoretical maximum density and bulk density of porous asphalt mixture were measured according to ASTM D2041, D3203, and D6857, respectively (Table 3.7).

Table 3.7. Density of porous asphalt mixture

Test items	Test result	Test method
Theoretical maximum specific gravity	2.560	ASTM D2041
Theoretical maximum density (g/cm^3)	2.553	ASTM D2041
Bulk density (g/cm^3)	1.919	ASTM D3203
	2.016	ASTM D6857

Air voids percentage was determined as 24.8%, according to ASTM D3203. Voids in coarse mineral aggregate of the compacted mixture (VCAmix) were measured to be 35.2% which is lower than that measured by dry-rodded technique (VCADRC=40.3%) (Table 3.8).

Table 3.8. Air voids of porous asphalt mixture

Test items	Test result	Test method
Percent Air Voids (%)	24.8	ASTM D3203
VCA of the compacted mixture (%)	35.2	ASTM D7064

Mechanical properties of the porous asphalt mixture were checked and are shown in Table 3.9.

Table 3.9. Compressive strength of porous asphalt mixture

No	Compressive strength/psi [MPa]	Mean
1#	391 [2.70]	366 [2.52]
2#	340 [2.34]	

Specimen size: φ100×100, load rate: 100 lb/s

Draindown Properties of Porous Asphalt Mixture

A sample of the asphalt mixture to be tested is prepared in the laboratory or obtained from field production. The sample is placed in a wire basket, which is positioned on a plate, or on another suitable container of known mass. The sample, basket, and plate or container are placed in a force draft oven for one hour at a pre-selected temperature. At the end of one hour, the basket containing the sample is removed from the oven along with the plate or container and the mass of the plate or container containing the drained material, if any, is determined (Figure 3.5). The amount of draindown is then calculated. The maximum permissible draindown should not exceed 0.3% by total mixture mass.

(a) (b) (c)

Figure 3.5. Images of draindown test

The draindown test is conducted on loose mixtures at 170°C and 185°C according to Test Method D6390. Results in Table 3.10 indicate that draindown amounts of porous asphalt mixture at both 170°C and 185°C meet the standard requirement.

Table 3.10. Draindown test results at different temperatures

	Draindown (%)	
Temperature (°C)	Standard requirement	Test result
170	≤0.3	0.165
185	≤0.3	0.18

Cantabro Abrasion Test Result of Porous Asphalt Mixture

At the discretion of the test designer, the porous asphalt mixture (PAM) may be tested by the Cantabro abrasion test to ensure adequate durability (Figure 3.6). Four samples sized at ϕ100mm×63.5mm are tested at the test temperature of 25°C. The drum speed is about 30 revolutions/min and a total of 300 revolutions are used in this test.

In semi-flexible pavement, porous asphalt mixture works in conjunction with cement to withstand vehicle loading. Thus, it is believed that abrasion loss is not an index that porous asphalt mixture should necessarily have to meet. Table 3.11 shows that both unaged and aged samples have higher abrasion loss values than standard requirements. Nevertheless, the design of this matrix is acceptable.

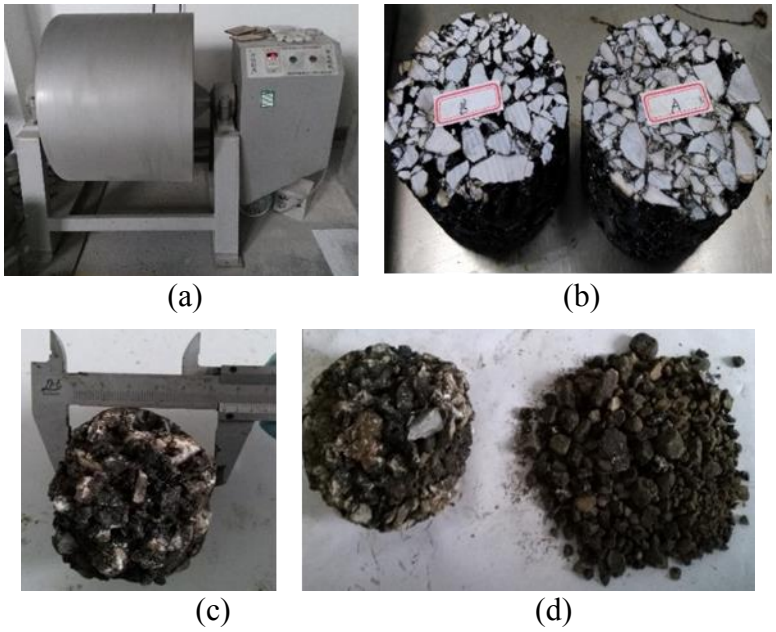

(a) (b) (c) (d)

Figure 3.6. Images of Cantabro abrasion test

Table 3.11. Abrasion loss of porous asphalt mixture

	Abrasion loss (%)	
Curing condition	Standard requirement	Test result
Unaged specimens	≤20	51.7
Aged specimens	≤30	73.0

Mix Proportion Design of Grout Material

Experimental Procedure for Grout Material

Mixing procedure—Water was weighed according to the mix ratio and the superplasticizer solution was prepared by mixing superplasticizer with a small portion of water. The 3,000g dry powder was placed in the mixing pot as shown in Figure 3.7(a), 80% of the water and superplasticizer solution were mixed with the dry powder after running the mixer at a low speed for 15 s. Then, the ingredients were mixed at medium speed for 2 min, followed by high speed for 1 min. Finally the remaining 20% of water was added to the mixing pot, and mixed into the paste at low speed for 1 min.

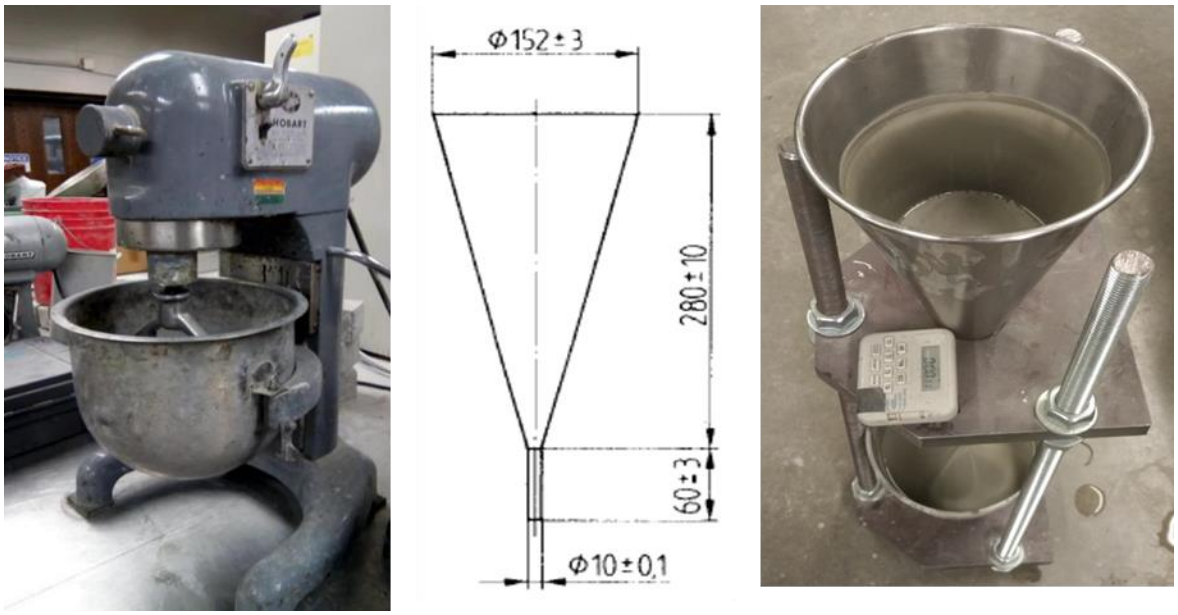

(a) Grout mixer (b) Measure of fluidity (c) Fluidity measurement

Figure 3.7. Fluidity test

The fluidity of paste test was performed according to ASTM C939, using a flow cone as shown in Figure 3.7(b) and (c). The method for measuring fluidity of paste is as follows: Prior to the test, the inner wall of the cone was moistened. The initial time when the bottom of the cone was open was recorded. Then the bottom of the cone was closed before putting 1,000 mL of the

cement paste into the cone. The time when the cement paste could no longer continuously outflow was recorded, which could be considered as the measure of fluidity.

Mix Proportion Selection of Grout Material

In order to achieve a uniform and dense CCAM, grouting materials should have the characteristics of high flow ability and high stability without segregation or water bleeding. In addition, to perform in severe climate conditions, high resistance freeze-thaw cycles and low shrinkage were required. Although entraining air bubbles is a good way to improve high freeze-thaw durability of grout, air bubbles entrainment was difficult to sustain for high-flowability, low-viscosity fresh grout. (This will be discussed in Section 4.4.) Therefore, in order to obtain high resistance freeze-thaw durability, a low water-binder ratio was required for grout material.

In this study, fly ash was utilized to improve the flowability of grout, and silica fume was utilized to improve the early strength and stability of grout. Mix proportions of grout material with various volume of fly ash and silica fume are listed in Table 3.12.

Table 3.12. Mix proportions and fluidity

Mix	Cement	Silica Fume	Fly Ash	W/B	Superplasticizer (ml/kg)*	SRA (ml/kg)
HSG-1	0.80	/	0.20	0.28	12	3
HSG-2	0.80	0.05	0.15	0.30	12	/
HSG-3	0.80	0.05	0.15	0.29	8	3
HSG-4	0.80	0.05	0.15	0.28	12	3

*Percent of total cementitious binder

The mix proportions of grout material were selected based on the test results of fluidity, water-binder ratio, and strength, which are presented in Table 3.13.

Table 3.13. Compressive strength

	Fluidity (s)		Compressive strength/psi [MPa]		
Mix	0 min	30 min	1 d	7 d	28 d
HSG-1	22	24	2,258[15.6]	6,380[44.3]	11,955[82.4]
HSG-2	22	25	2,584[17.8]	5,978[41.2]	10,766[74.2]
HSG-3	23	24	4,168[28.7]	9,268[63.9]	11,427[78.8]
HSG-4	31	35	2,975[20.5]	8,950[61.7]	10,512[72.5]

Figure 3.8 presents the variations of compressive strength at 1 d, 7 d, and 28 d, respectively. It can be seen that the highest compressive strength is 28.7 MPa (4168 psi) at 1 d corresponding with HSG-3, while the lowest compressive strength is only 15.6 MPa (2258 psi) at 1 d corresponding with HSG-1.

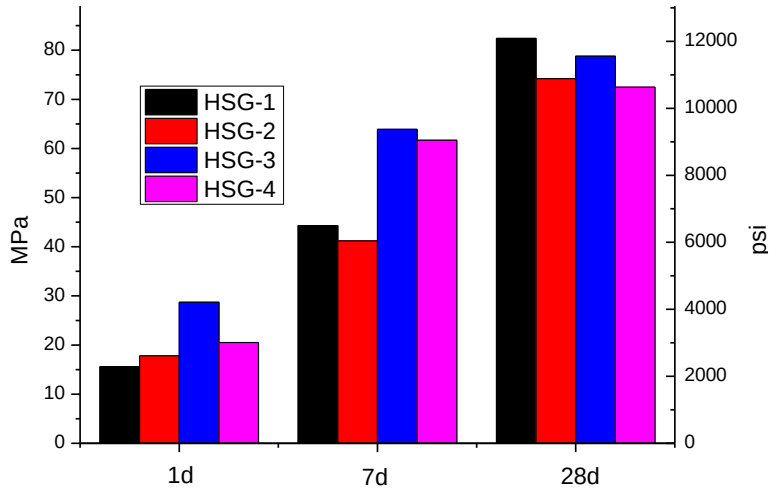

Figure 3.8. The variation of compressive strength at different ages

The gap in compressive strength between HSG-1 and HSG-3 could be attributed to these factors: the compressive strength measure is dominated by the cement hydration and the microstructure of cement paste. For the HSG-1 mix, only fly ash was incorporated into the cement paste, while part of the fly ash was replaced by silica fume for the HSG-3 mix. As has been shown, the reactivity of silica fume is higher than that of fly ash during early stages; that is, more hydration products and a denser structure tend to be formed with the addition of silica fume. Therefore, the compressive strength of HSG-3 is higher than that of HSG-1. When comparing HSG-2 with HSG-3, the compressive strength of HSG-3 at different ages was much higher, which is mainly due to the lower ratio of W/B.

The amount of superplasticizer in the HSG-4 mix is higher than that of the HSG-3 mix. The presence of more superplasticizer led to segregation and water bleeding, which exerted an adverse effect on the formation of the microstructure and the compressive strength, in spite of the lower ratio of W/B in the HSG-4 mix. This could explain why the compressive strength of HSG-4 is lower than that of HSG-3.

After consideration of its early strength at 1 d and the development of compressive strength at a later age, the HSG-3 mix ratio was selected as the optimal mix proportion.

PROPERTIES OF HYBRID CONCRETE

Preparation of Test Specimens

The CCAM was produced by pouring grout mixture onto the surface of open graded asphalt skeletons. Slabs with a size of 75 mm×210 mm×380 mm, and samples with a diameter of 100 mm and height of 100 mm or 150 mm were prepared. Slabs and cylinder samples were cut into different sizes for different tests. An adequate, constant supply of grout materials was prepared to ensure that voids in the asphalt mixture were completely filled. At the end of the grouting process, a brush was used to scrape off the excess grouting material until the surface of asphalt mixture was exposed. The grouted asphalt mixtures were cured in a room at 25°C and 75% relative humidity for 48 h (Figure 4.1).

(a) Asphalt mixture samples

(b) Pouring grouting materials

(c) CCAM cylinder sample

(d) CCAM slab sample

Figure 4.1. CCAM preparation process

Information on grout type and admixtures used is listed in Table 4.1. The experimental plan is also given.

Table 4.1. Details of different samples for test

Mixes	Grout type	Admixture	Test item		
			Mechanical properties	Shrinkage	Freeze-thaw
CCAM-ESG	ESG	/	√	√	√
CCAM-ESG-SRA		SRA	√	√	/
CCAM-ESG-AEA		AEA	√	/	√
CCAM-HSG	HSG	SRA	√	√	√

Mechanical Properties

Compressive Strength

Specimens sized at 100 mm by 100 mm are prepared. The specimens are tested in axial compression without lateral support at a uniform rate of vertical deformation of 5 mm/min. Specimen failure is defined as the maximum load experienced by the specimen during the compression process (AASHTO T 167-10). The details of compressive testing and failed specimens are shown in Figure 4.2.

Figure 4.2. Compressive strength test and failed samples

Compressive strength of different CCAM samples, grouting materials, and asphalt mixtures is shown in Table 4.2.

Table 4.2. Compressive strength of different samples

Mix	Compressive strength/MPa		
	7d	14d	28d
CCAM-ESG	4.07	5.05	4.67
CCAM-ESG-SRA	4.74	4.96	4.61
CCAM-HSG	4.21	4.83	5.41
ESG	26.2	28.0	29.5
HSG	63.9	70.2	78.8
PAM	2.52	2.52	2.52
AC13*	1.7–3.8	1.7–3.8	1.7–3.8

*ASTM D6390 and Cai et al. 2017

It was found that grouting materials show much higher strength than asphalt mixtures. However, the CCAM, which consists of both grouting material and an asphalt mixture, exhibits only slightly higher strength than the asphalt mixture, while its compressive strength is much lower than that of grouting materials. It can be seen that the addition of grouting material can increase the overall strength of asphalt mixture. The CCAM's strength was also found to be higher than that of the AC13 mixture. This reveals that filling the voids with rigid materials would make the mixture much stiffer than that with viscoelasticity materials. Even though the ESG and HSG have dramatically different compressive strength, the CCAM-ESG and CCAM-HSG mixtures show similar compressive strength. This indicates that the weak zone in the CCAM lies in the asphalt layer. Addition of grouting materials would change the skeleton structure, which would increase the CCAM's strength. However, the stiffness of grouting materials may contribute little to the overall strength of the CCAM when their stiffness is higher than that of the typical asphalt matrix.

Compressive strength data were used to calculate the contributive efficiency rates of grouting materials and asphalt matrices, respectively (Cai et al. 2017). Results are illustrated in Figure 4.3 and Figure 4.4.

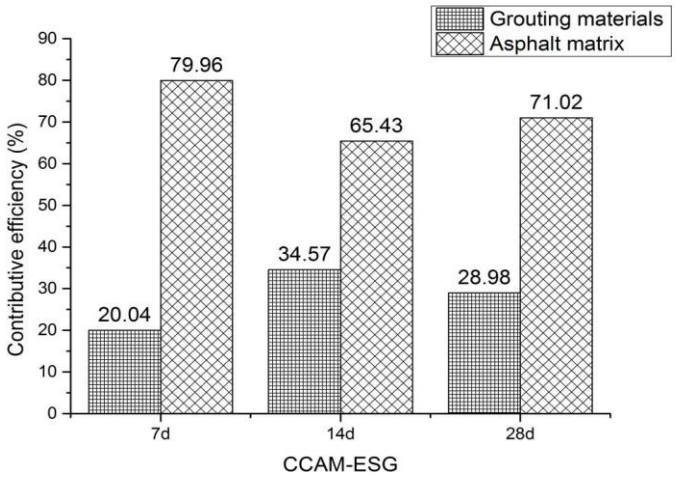

Figure 4.3. Contributive efficiency of grouting material and asphalt matrix in CCAM-ESG

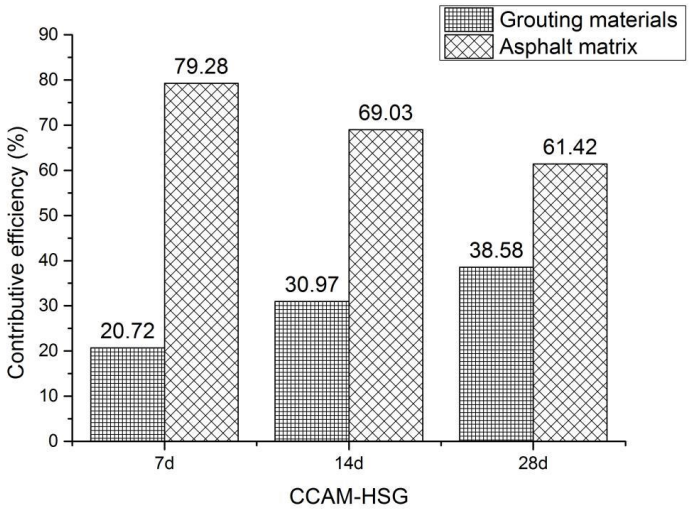

Figure 4.4. Contributive efficiency of grouting material and asphalt matrix in CCAM-HSG

It was demonstrated that the asphalt matrix has a decisive effect on the compressive strength of the CCAM with a contributive efficiency ranging from 60% to 80%. It was found that the contributive efficiency of grouting material became higher as the curing period increased, except for the CCAM-ESG sample that was cured for 28 days. The findings in this project are consistent with those in the literature. Cai et al. (2017) also found that the contributive efficiencies of grouting material and matrix asphalt to the compressive strength of the CCAM are about 40% and 60%, respectively. Indirect Tensile Strength and Deformation

The indirect tensile test (IDT) temperature was set at 25°C. Each specimen was placed in the environmental chamber at the test temperature for 3 h prior to testing. The tensile strength was determined by applying a vertical load to the specimen at the rate of 10 mm/min (Figure 4.5).

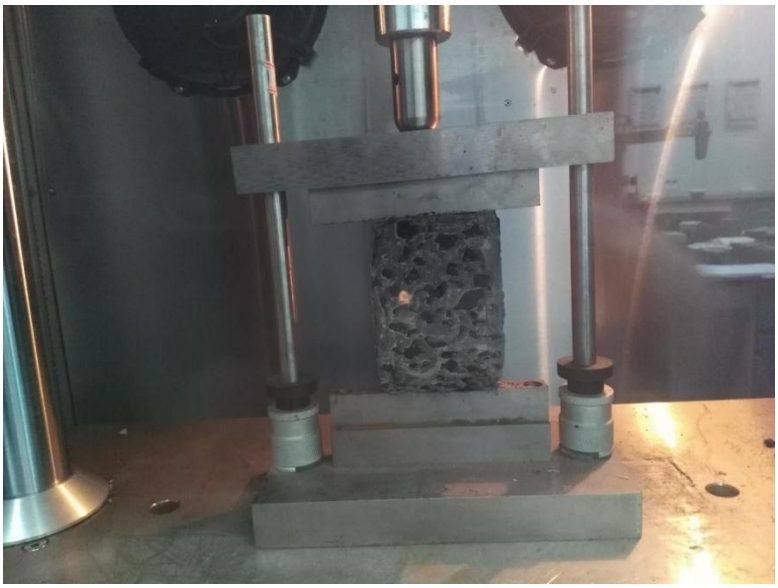

Figure 4.5. IDT test

The vertical and horizontal deformations on both ends of the specimen, together with the loads, are recorded (Figure 4.6) until the load starts to decrease (AASHTO T 322-07).

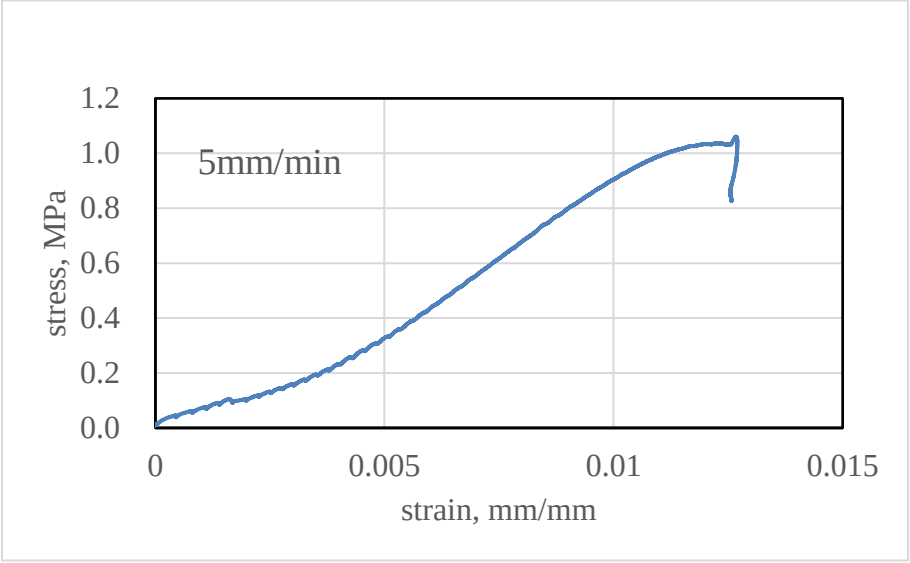

Figure 4.6. Strain-stress curve of IDT test

The IDT strengths of different samples are listed in Table 4.3. A higher loading rate corresponds to higher IDT strength. It was found that the IDT strength of the CCAM-HSG measured with a loading rate of 10 mm/min is lower than that of the CCAM-ESG measured with a loading rate of 5 mm/min. Thus, it is speculated that the CCAM-HSG has lower IDT strength than the CCAM-ESG at same loading rate. Since the same aggregate and asphalt binder were used, it is believed that the adhesion between asphalt and grouting material in the CCAM-ESG is better than that in the CCAM-HSG.

Table 4.3. Indirect tensile strength

No.			IDT strength (MPa)	Peak load strain (%)
CCAM-ESG	Loading rate (mm/min)	50	1.40	1.2
		5	0.94	1.4
CCAM-HSG	Loading rate (mm/min)	10	0.82	0.47

Resilient Modulus

The resilient modulus of the CCAM-HSG was measured according to JTG E20 T 0713-2011, Standard Test Methods of Bitumen and Bituminous Mixtures for Highway Engineering (Research Institute of Highway 2011). A load was applied on the CCAM sample with a loading rate of 2 mm/min until the sample failed. The peak-force (P) was recorded and used to determine the loading level in a subsequent resilient modulus test (Figure 4.7).

Figure 4.7. Resilient modulus test

Seven loading levels (from 0.1 P to 0.7 P) were used and the resilient deformations are plotted in Figure 4.8. The regressed deformation value at 0.5 P was extracted to calculate the resilient modulus.

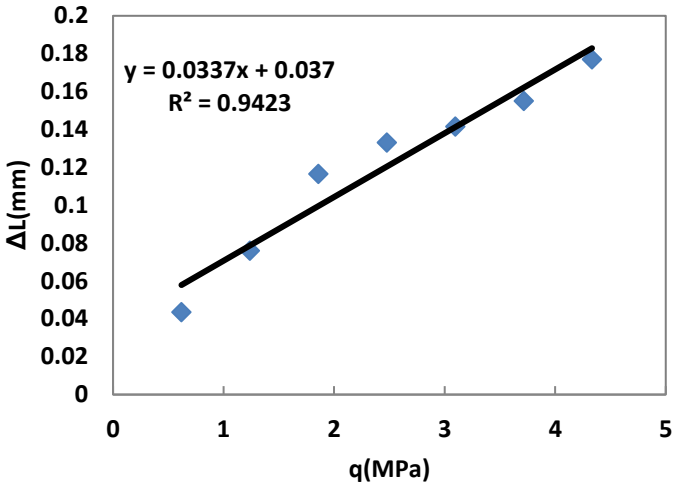

Figure 4.8. Regression of resilient deformation

Resilient modulus test results are listed in Table 4.4. It was shown that the CCAM has a resilient modulus two times higher than the AC-13 mixture. These results again prove that the CCAM is stiffer than a traditional asphalt mixture.

Table 4.4. Resilient modulus test result

Mixture	Peak force (kN)	Strength (MPa)	Resilient modulus (MPa)
CCAM	49.37	6.19	1,761.64
AC13	-	4.20	726.3

Rutting Resilience

Performance results for the CCAM were evaluated by a wheel tracking test according to JTG E20-2011 T0719-2011. The performance test applied to the 300 mm×300 mm×50 mm slab at 60°C was set as 0.7 MPa. A wheel traveled back and forth on the surface of the slab for 1 h. A total of 2,520 cycles was performed. The rut-depth curves of the CCAM-ESG, CCAM-HSG, HMAC, and AC were recorded as shown in Figure 4.9.

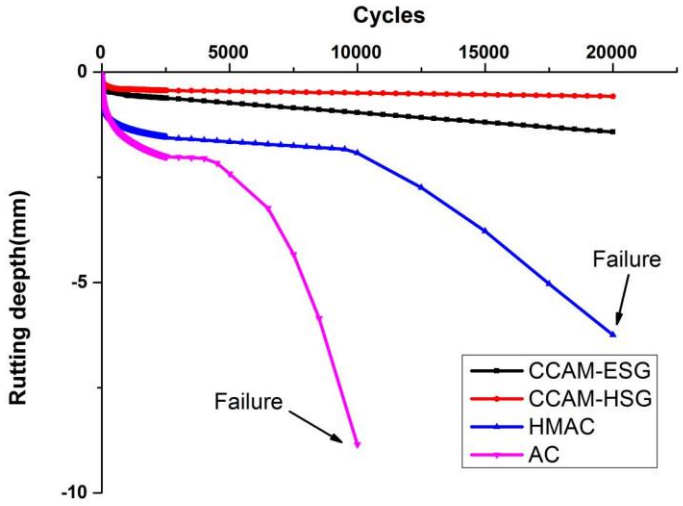

AC=asphalt concrete, HMAC=high modulus asphalt, ESG=early set grout, HSG=high strength grout

Figure 4.9. Rut depth curve of the CCAM-ESG, CCAM-HSG, HMAC, and AC

Figure 4.9 shows that the CCAM exhibits better rutting performance than asphalt concrete (AC) and high modulus asphalt concrete (HMAC). Though the CCAM-ESG and the CCAM-HSG have similar compressive strength, the CCAM-HSG shows lower rut depth than the CCAM-ESG, which indicates that HSG can enhance the rutting performance of the CCAM more significantly. The difference between the compressive test and wheel tracking test results lies in the loading mode and figuration of tested samples. No confining pressure was induced in the compressive test, while a confining pressure exists along the wheel track within the slab. Thus, the failure mode varies in different tests. In the compressive test, the main degradation is the failure of adhesion between aggregate/cement and asphalt mastic or the cohesion within asphalt mastic itself, while the main degradation in the rutting slab is the failure of its skeleton. HSG with higher modulus would fill in the voids of the asphalt matrix skeleton, which would make the whole mixture stiffer. This enhancement would result in decreased rutting in the CCAM-HSG.

The dynamic stability (DS) of the concretes tested is determined from the rutting test data at 45 min and 60 min, and the results are shown in Table 4.5.

Table 4.5. Dynamic stability of CCAM-HSG

D_1 (mm)	D_2 (mm)	DS (cycle/mm)
0.428	0.436	78750

The DS of CCAM is dramatically higher than that of traditional asphalt mixture. Higher DS value corresponds to better rutting performance. This indicates that CCAM rates much better

than asphalt mixture in rutting performance. The CCAM slab that was tested is shown in Figure 4.10.

Figure 4.10. Rut depth of a CCAM slab

Almost no rut can be found on this slab. One interpretation of this phenomenon is that the modulus of grouting material in the voids of skeleton is not temperature-dependent. The existence of rigid material with high modulus makes the CCAM stiff at a high temperature where no plastic deformation can be found in the mixture.

Tensile Strength Ratio

Test specimens with a 100 mm diameter and 63 mm height were prepared using a gyratory testing machine. Each set of specimens was divided into subsets. One subset was tested in dry conditions for indirect-tensile strength. The other subset was subjected to vacuum saturation and a freeze cycle, followed by a warm-water soaking cycle, before being tested for strength measurements (AASHTO T 283-07 2011).

The typical strain-stress curves for unconditioned and conditioned samples are shown in Figure 4.11.

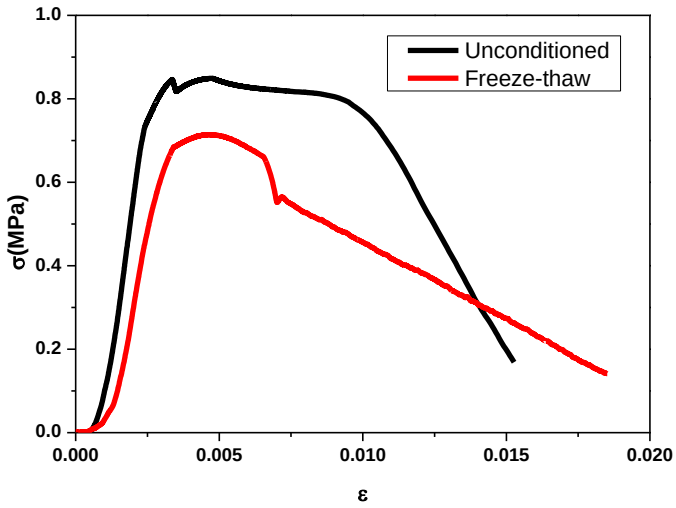

Figure 4.11. Strain-stress curve of unconditioned and conditioned CCAM-HSG samples

Figure 4.11 shows that the unconditioned sample has a higher peak-strain value than the conditioned one. This indicates that the freeze-thaw process degrades the structure as well as the strength of the CCAM. Results of moisture sensitivity tests on CCAM samples are illustrated in Table 4.6.

Table 4.6. Tensile strength ratio of CCAM-HSG samples

	Height (mm)	Peak-strain value	Strength (MPa)	TSR (%)
Unconditioned	63.68	0.0047	0.85	85.68
Conditioned	66.47	0.0052	0.73	

The CCAM-HSG sample is found to have a tensile strength ratio (TSR) value higher than 80%, which shows it possesses fairly good anti-moisture properties.

Free Drying Shrinkage

The free drying shrinkage properties of grouting materials ESG, HSG, and CCAM were studied. The CCAM was prepared using ESG and HSG. SRA was separately incorporated into ESG grouting material and the CCAM to investigate its influence on free-drying shrinkage. As for HSG, only HSG grouting material was affected by the SRA.

The test of free drying shrinkage was in accordance with ASTM C157/C157M-08. Three specimens were prepared for each mixture type. The test specimens for ESG and HSG were prisms of 1-in. (25-mm) square cross-sections approximately 11 in. (285 mm) in length. The prisms of 3 in. (75mm) square cross-sections approximately 10 in. (250mm) in length were cut

from the CCAM slabs at about 20 h after casting the grouting into the porous asphalt mixture slabs. Then the gage studs were stuck to the center of the specimens at both ends (Figure 4.12).

(a) GM specimens (b) CCAM specimens

Figure 4.12. Drying shrinkage samples

The prisms' initial length comparator reading were recorded at 24h±1⁄2h after the addition of water to the cement during the mixing operation. Then the prisms were placed in a moist curing room for seven days. After seven days, the prisms' lengths were measured. The prisms were then stored in a drying room, at a temperature of 73±3°F with relative humidity of 50±4%, for subsequent measurements. Additional length measurements were obtained at 3, 7, 14, and 28 days.

The calculated percent change in length were presented in two ways: the changes due to drying only and the changes due to moist curing and drying, which showed the swelling behavior of the mixes during moist curing or wetting. Figure 4.13 and Figure 4.15 show the total length changes that include the moist curing and drying periods. Figure 4.14 and Figure 4.16 show the percent length changes during drying.

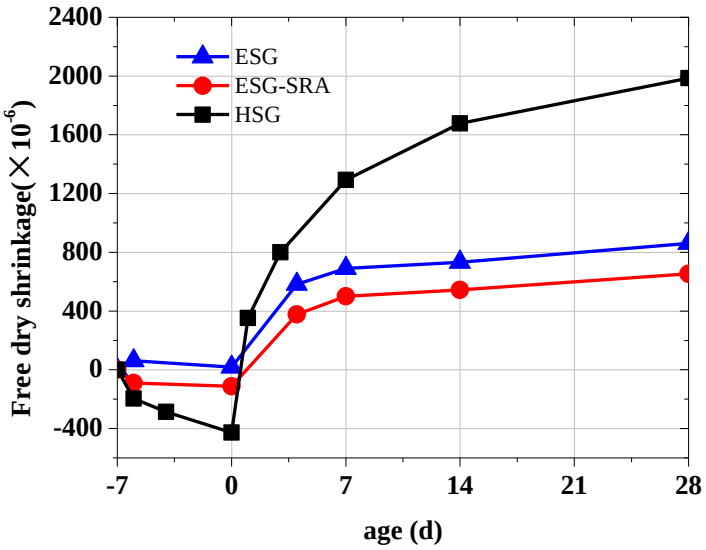

Figure 4.13. Total change in length due to moist curing followed by free drying shrinkage of the ESG, ESG-SRA, and HSG

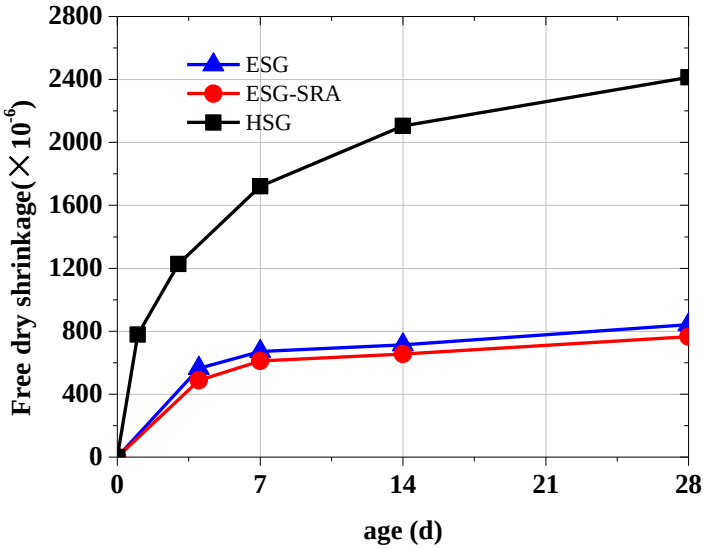

Figure 4.14. Length change due to free drying shrinkage of the ESG, ESG-SRA, and HSG

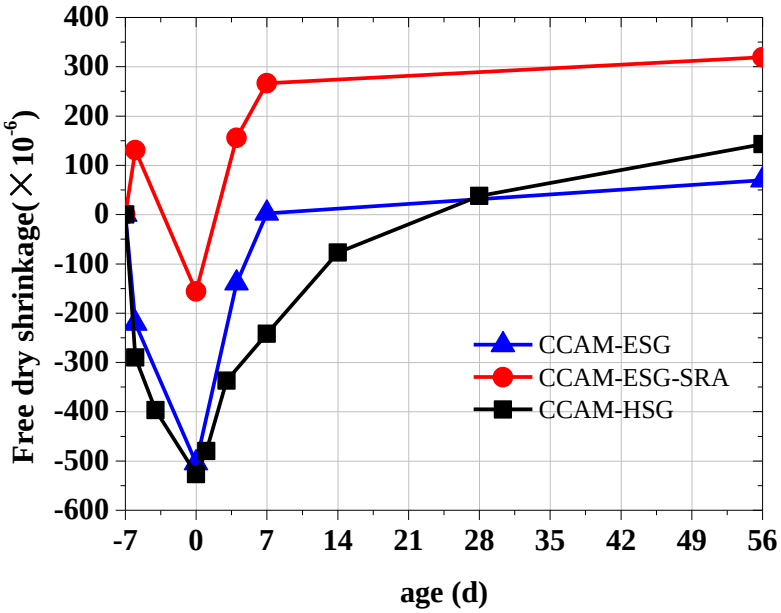

Figure 4.15. Total change in length due to moist curing followed by free drying shrinkage of the CCAM-ESG, CCAM-ESG-SRA, and CCAM-HSG

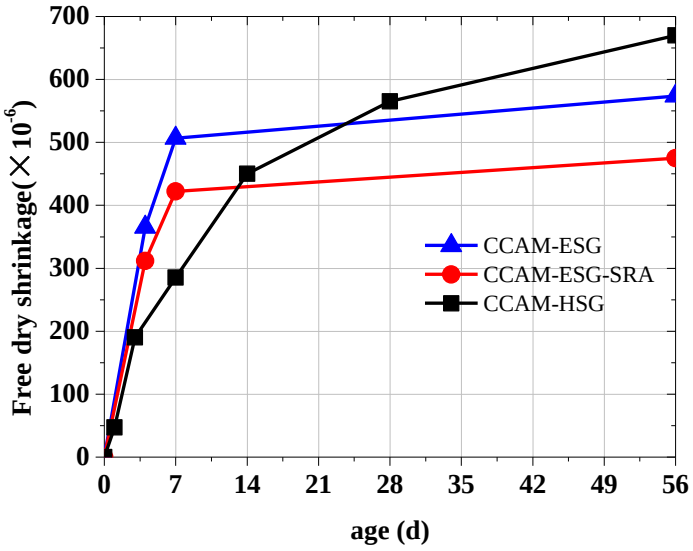

Figure 4.16. Length change due to free drying shrinkage of the CCAM-ESG, CCAM-ESG-SRA, and CCAM-HSG

Figures 4.13 through 4.16 indicated there was significantly greater free drying shrinkage of grouting material HSG in comparison with ESG. At 28 days, the free drying shrinkage of HSG was about 3 times larger than that of ESG. The 5% silica fume and lack of fine aggregates in HSG were two main contributing factors.

CCAM-HSG had relatively greater free drying shrinkage compared with CCAM-ESG and CCAM-SRA, but it was only a marginal increase. This was due to the inhibiting effect of PAM, the CCAM's skeleton, in which the coarse aggregates formed interlocking dense structures. The SRA contributed to reducing the free drying shrinkage of the grouting material, but only on a limited scale.

The elastic modulus and strength of the CCAM were low. Compared with ordinary concrete, its resistance or restraining effect on shrinkage was weaker than that of aggregates, resulting in slightly greater free drying shrinkage in the CCAM. Although CCAM shrinkage was larger, its shrink stress response was smaller than for concrete, also owing to the low elastic modulus. Accordingly, the scientific evaluation for crack resistance of the CCAM should comprehensively consider factors such as material strength, elastic modulus, free drying shrinkage, and autogenous shrinkage. The cracking risk estimation also needs further study.

Freeze-Thaw Durability

The freeze-thaw durability of the PAM, ESG, HSG, CCAM-ESG, CCAM-ESG-AEA, and CCAM-HSG to cyclic F-T was measured according to ASTM C666, Method B. Relative dynamic modulus of elasticity and mass loss as damage were used as evaluation indicators. Prism failure was considered to occur when the relative dynamic modulus of elasticity reached

60% of the initial modulus or the mass loss reached 5%. Two 3×4×16 in. prisms were prepared for each mix. Of the six mixes, only the CCAM-ESG-AEA was air entrained. The prisms were moist cured for 28 days before being subjected to F-T cycles. The tests were conducted until the relative dynamic modulus of elasticity was below 60% or the mass loss was beyond 5%, whichever occurred first. Otherwise, the test procedure ended when 300 cycles were reached. The durability factor, mass loss, and images of the prisms after the test are shown in Figure 4.17 through Figure 4.25.

As shown in Figure 4.17, along with the accumulation of freeze-thaw cycles, the relative dynamic modulus of elasticity of PAM declined sharply while the mass loss increased continuously.

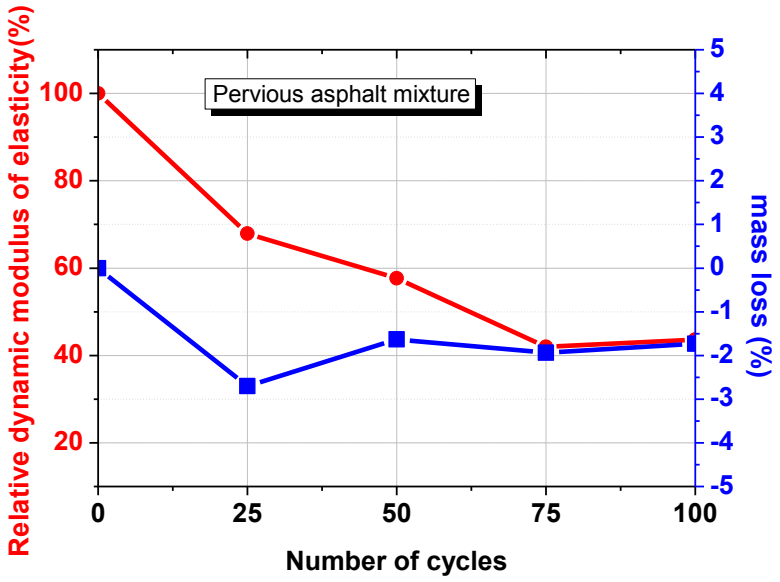

Figure 4.17. Relative dynamic modulus of elasticity and mass loss of PAM

When the freeze-thaw cycle reached 25 and 50 times, the relative dynamic modulus was lower than 70% and 60%, respectively. After 25 freeze-thaw cycles, the mass loss of the PAM was close to 3%. When the number of cycles reached 50, PAM had an increased mass because specimens with freeze-thaw damage could absorb water to compensate for some of the loss. The mass loss of PAM specimens tended to be stable during the latter 50 cycles.

Figure 4.18 shows that no obvious appearance change was observed when the PAM underwent fewer than 50 cycles.

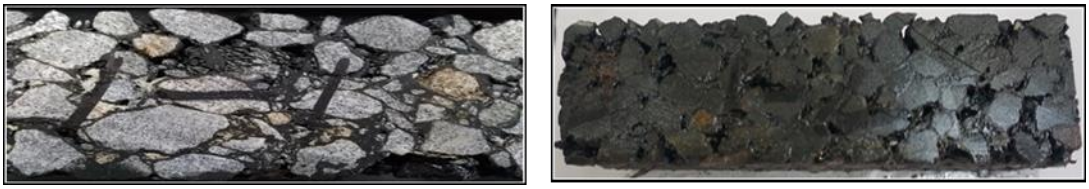

(a) 0 F-T cycle (b) 50 F-T cycles

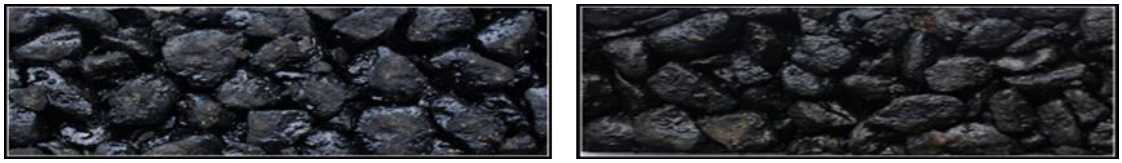

(c) 75 F-T cycles (d) 100 F-T cycles

Figure 4.18. PAM after different F-T cycles

When the number of cycles exceeded 75, asphalt film on the surface of the specimens gradually peeled from the aggregates.

Consequently, the freeze-thaw resistance time of PAM was 25 times, which illustrated its quite weak freeze-thaw resistance capacity, according to the ASTM C666 rapid freezing and thawing experiment method. The specimen failure mechanism was summarized in two ways. First, the void fraction of PAM exceeded 20% and the expansion of water in the gaps caused internal damage or cracking of the specimens. In addition, water would penetrate to the asphalt aggregate interface during the freeze-thaw process, which would lead to peeling of the asphalt membrane.

The relative dynamic modulus of elasticity and mass loss of ESG are illustrated in Figure 4.19.

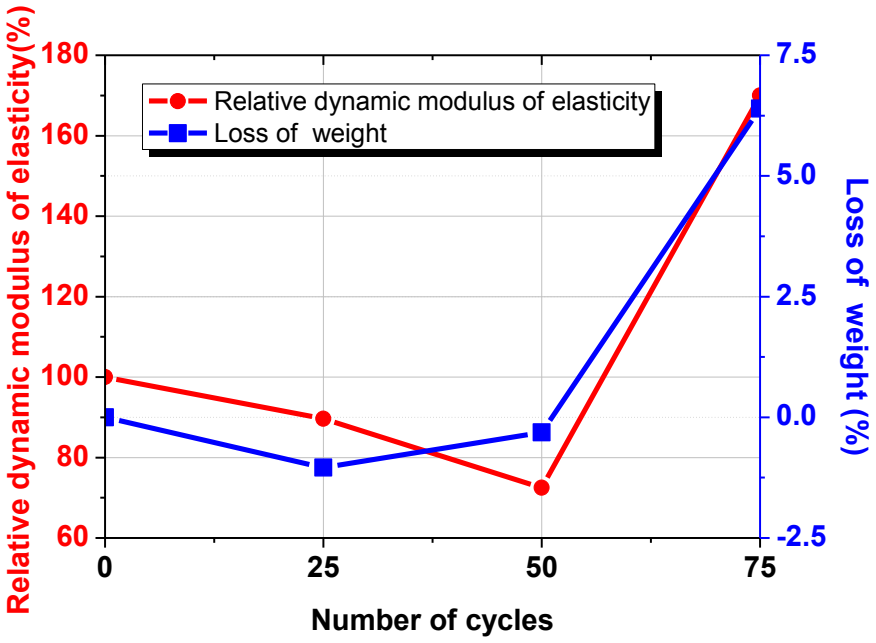

Figure 4.19. Relative dynamic modulus of elasticity and mass loss of ESG

When freeze-thaw cycles were performed less than 50 times, the relative dynamic modulus of elasticity for ESG decreased rapidly as the cycle times increased. Meanwhile, the mass loss of ESG had a tendency to increase first and then decline. When the number of freeze-thaw cycles was between 25 and 50, the relative dynamic modulus of elasticity approached 90% and 70%, while the mass loss was within 1.25% and 0.5%, respectively. However, it was observed that when the freeze-thaw process reached 75 cycles, the relative dynamic elastic modulus sharply increased while the mass loss decreased drastically.

Figure 4.20 showed serious damage of specimens after 50 freeze-thaw cycles and ESG was severely damaged after it underwent 75 cycles.

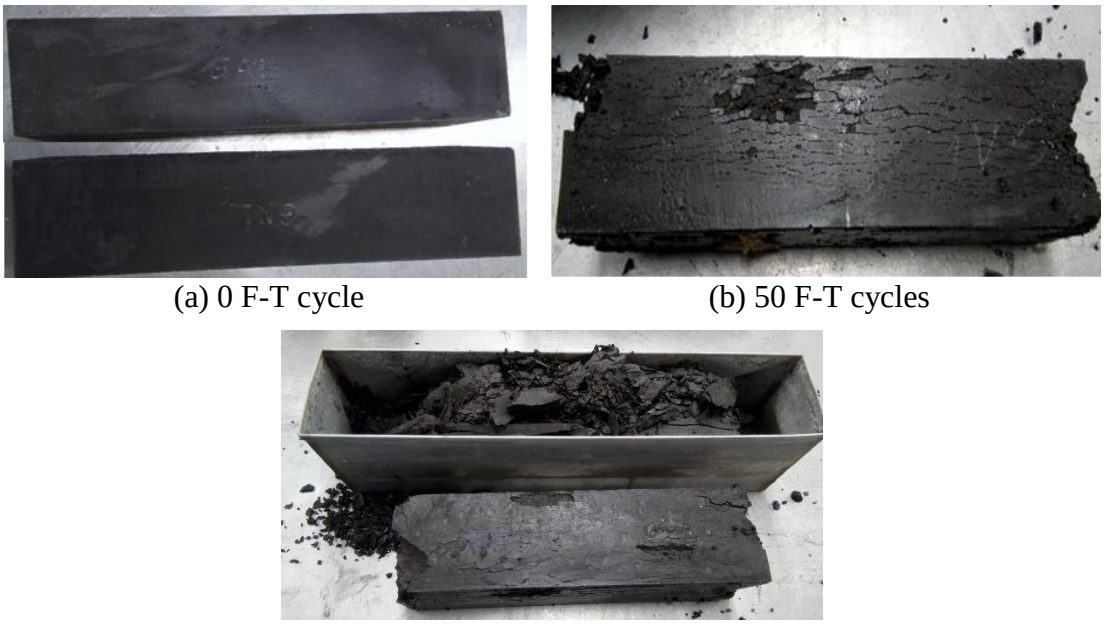

(a) 0 F-T cycle (b) 50 F-T cycles

(c) 75 F-T cycles

Figure 4.20. ESG after different F-T cycles

Based on the appearance changes of the specimens, it could be estimated that the freeze-thaw number of ESG was no more than 50. The relative dynamic elastic modulus may have increased at 75 cycles due to data distortion. It was rather difficult to measure the experimental data when the specimen was seriously damaged. Prisms that gained increased mass did so mainly because a large amount of water was absorbed.

In summary, the freeze-thaw resistance time of ESG was smaller than 50 cycles according to results of relative dynamic elastic modulus and mass loss tests, and the deteriorating appearance of the specimens. Lack of material strength and air-entraining led to the weak freeze-thaw resistance capability of ESG, which was mainly applied for use in a non-cold area in engineering practice.

Figures 4.21 through 4.23 showed the results of relative dynamic elastic modulus and mass loss tests of the CCAM prisms infused with ESG (CCAM-ESG).

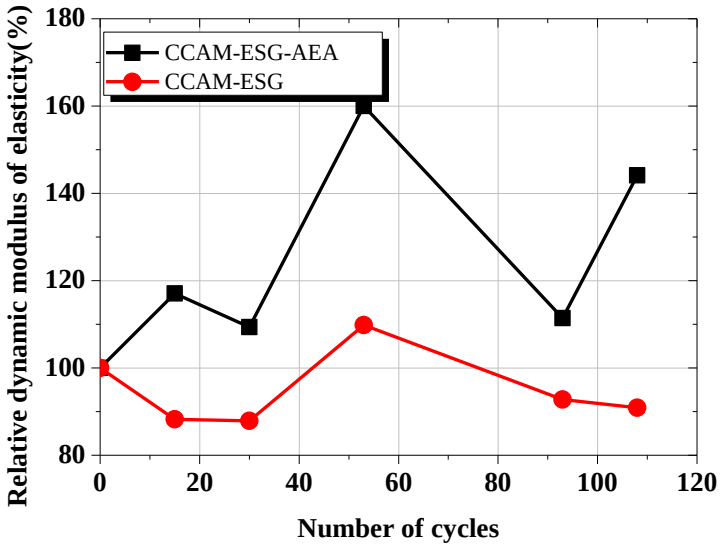

Figure 4.21. Relative dynamic modulus of elasticity of the CCAM-ESG-AEA and CCAM-ESG

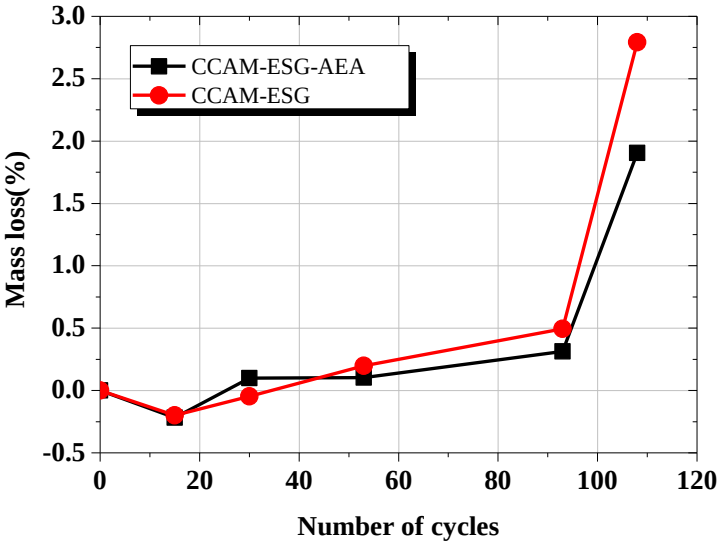

Figure 4.22. Mass loss of the CCAM-ESG-AEA and CCAM-ESG

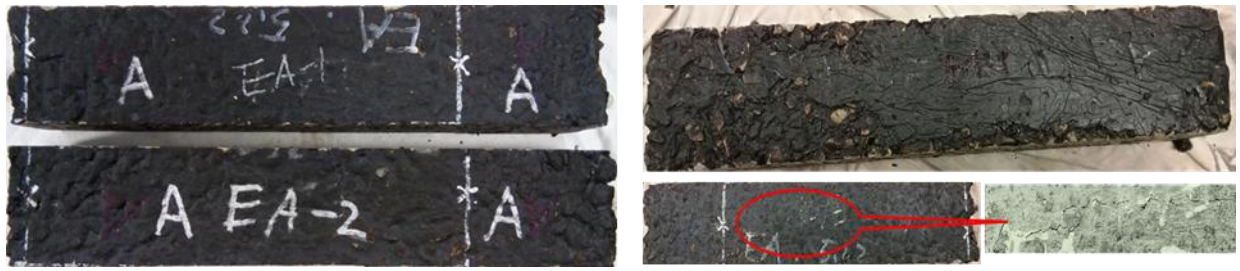

(a) 0 F-T cycles (b) 53 F-T cycles

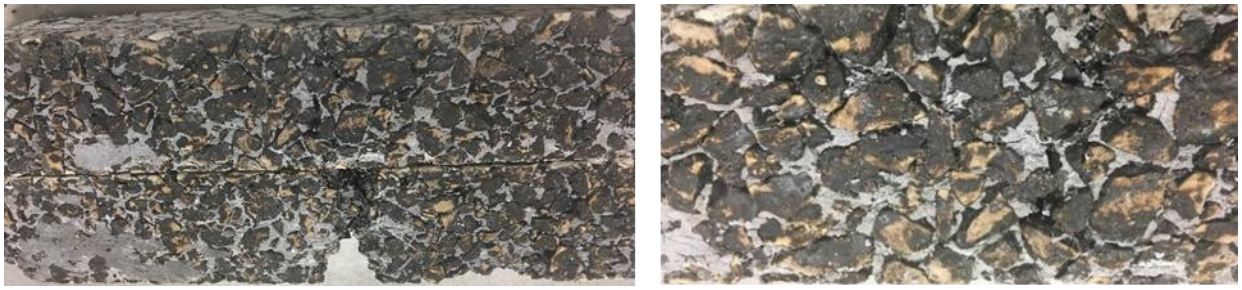

(c) 108 F-T cycles (d) 108 F-T cycles

Figure 4.23. The CCAM-ESG after different F-T cycles

The appearance changes of the CCAM-ESG are shown as well. Experimental results indicated that ESG and PAM both had relatively weak freeze-thaw resistance capacity. Previous studies proved that air entraining was an effective way to improve the frost resistance of cement concrete. In order to improve the frost resistance of the CCAM, an air-entraining agent was added to ESG, which could introduce bubbles into the material. The frost resistance of the CCAM-ESG-AEA was studied.

Figure 4.21 and Figure 4.22 indicate that the development process of the CCAM-ESG was similar to that of ESG. Figure 4.23 shows the appearance of specimens under various cycles of freeze-thaw tests. Visible cracks appeared on the surface of the CCAM-ESG after 50 cycles. When the freeze-thaw cycles exceeded 100 times, the CCAM-ESG specimen was fractured and most of the asphalt film was peeled off. Therefore, the CCAM-ESG could only bear fewer than 50 freeze-thaw cycles.

Compared with CCAM-ESG, the CCAM-ESG-AEA had slightly improved freeze-thaw resistance ability. The main reason was that the strong fluidity and low viscosity of ESG significantly benefited the process of bubble overflow.

Figure 4.24 shows that in the initial 150 freezing and thawing cycles the relative dynamic modulus of elasticity of HSG declined somewhat, but decreased dramatically when the freeze-thaw cycle accumulated over 150 times.

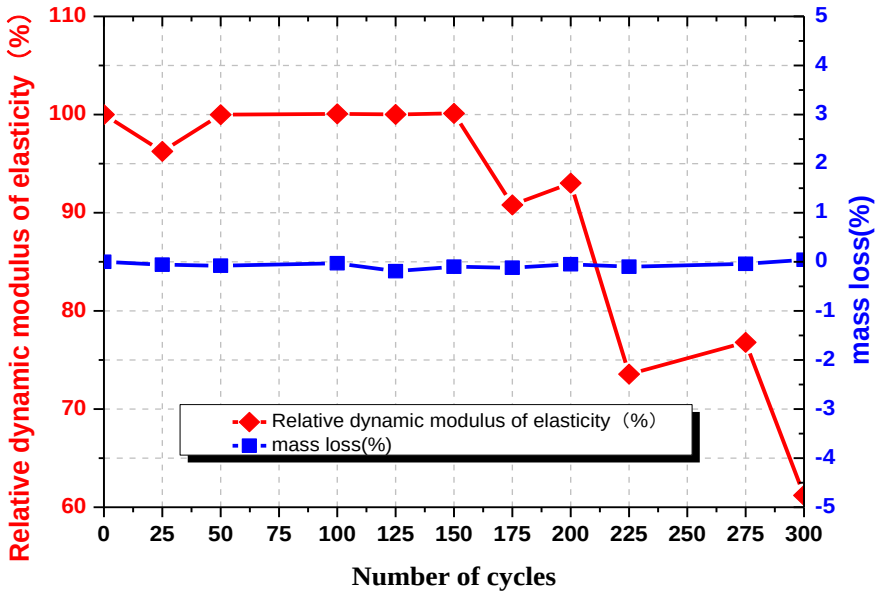

Figure 4.24. Relative dynamic modulus of elasticity and mass loss of HSG

Meanwhile, there was not an obvious change of mass loss. As a result of 300 freeze-thaw cycles, the relative dynamic modulus of elasticity decreased to 60% and the mass loss was less than 0.2%.

From Figure 4.25, it was observed there was no significant change in the surface of the HSG as the number of cycles increased continuously.

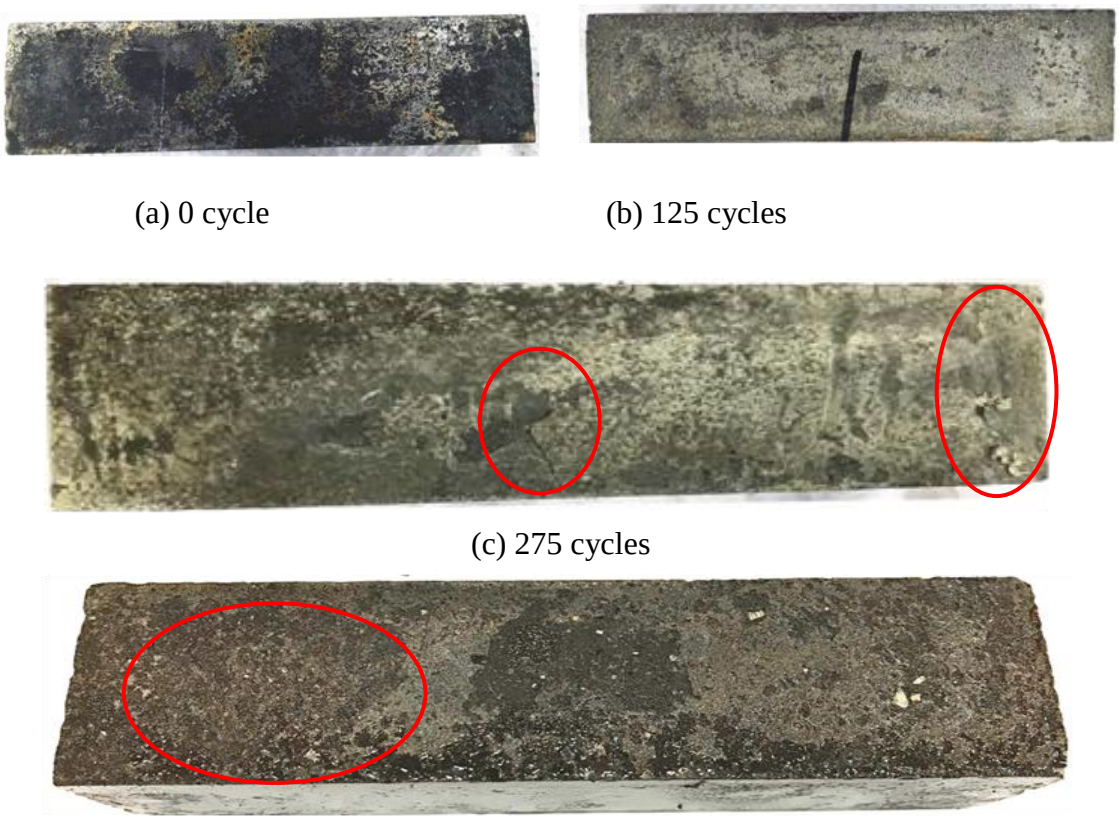

(a) 0 cycle (b) 125 cycles

(c) 275 cycles

(d) 300 cycles

Figure 4.25. HSG after different F-T cycles

The surface of HSG had only minor evidence of peeling and loosening after 275 cycles. There was slight peeling on the surface course, but there was no obvious damage after the specimen underwent 300 cycles. This observation highlighted the great freeze-thaw resistance capacity that HSG had.

Figure 4.26 indicates that in the initial 100 freeze-thaw cycles, the relative dynamic elastic modulus of the CCAM-HSG varied a little and the mass loss slightly decreased.

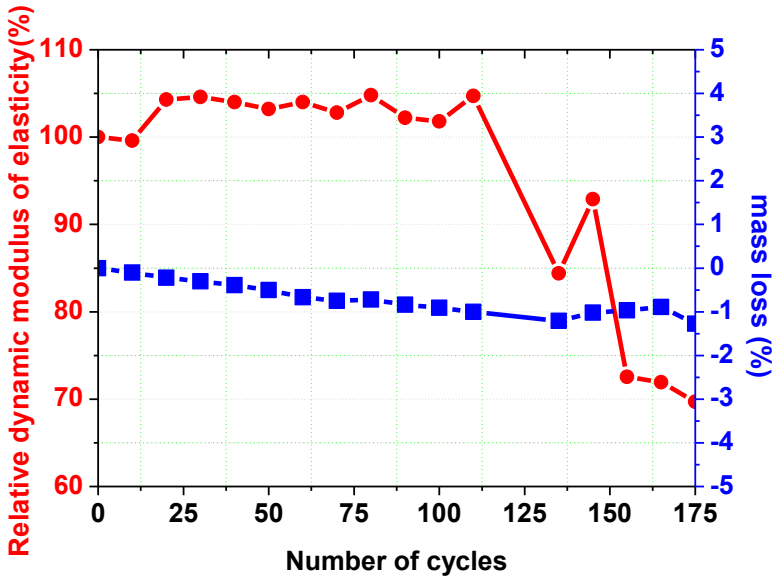

Figure 4.26. Relative dynamic modulus of elasticity and mass loss of CCAM-HSG

When the number of freeze-thaw cycles reached 100, mass loss was lower than 1%. After 100 freeze-thaw cycles, the relative dynamic modulus of elasticity decreased rapidly while the mass loss remained steady. The prism subjected to 175 cycles had a mass loss lower than 1.5%, but its relative dynamic modulus of elasticity declined below 70%.

Figure 4.27 shows that the surface of the CCAM-HSG gradually peeled a little when the number of freeze-thaw cycles increased.

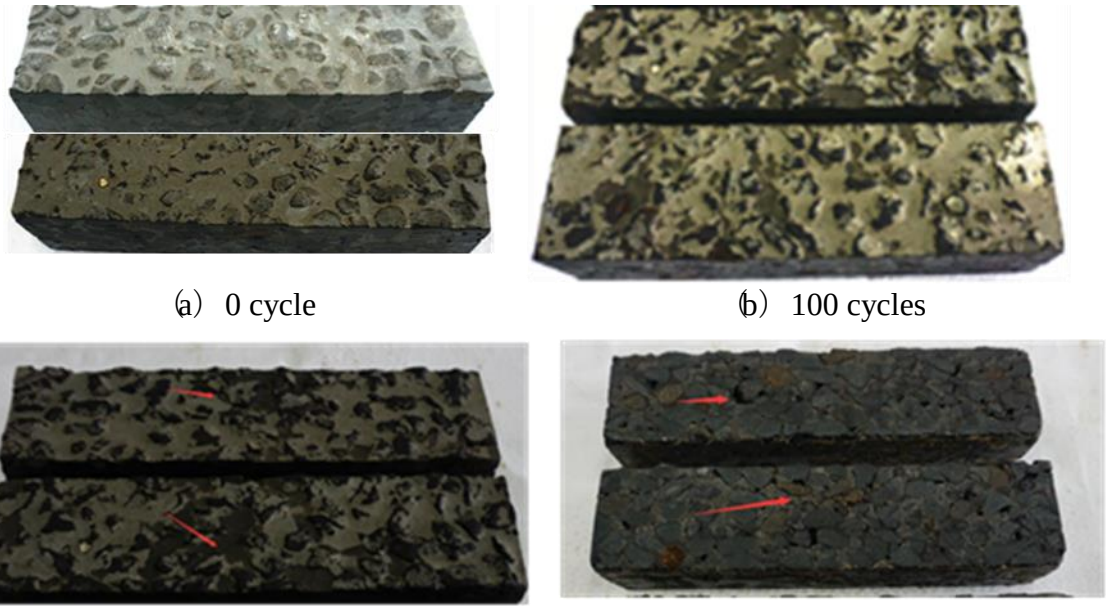

(a) 0 cycle (b) 100 cycles

(c) 175 cycles (d) 175 cycles

Figure 4.27. CCAM-HSG after different F-T cycles

No apparent damage was found and no peeling of the asphalt membrane was observed even after 175 cycles. It could be concluded that the CCAM-HSF had an enormous enhanced freeze-thaw resistance capacity.

The number of CCAM-HSG freeze-thaw cycles was more than 175, based on the results of relative dynamic modulus of elasticity and mass loss of the CCAM-HSG as well as appearance changes.

On the basis of the results and analyses of the PAM, ESG, HSG, and CCAM for their freeze-thaw resistance properties with different types of grouting material, the main conclusions were summarized as follows:

1. Because of the poor frost resistance of PAM and ESG, the freezing resistance capacity of the CCAM-ESG was also relatively low. Due to the low viscosity of ESG, it was difficult to encapsulate air bubbles. It was not feasible to improve its resistance ability by adding an air-entraining agent.

2. HSG had a low water to binder ratio and high strength, so its freeze-thaw resistance capacity was significantly greater than for ESG. The number of freeze-thaw cycles of the CCAM with grouting material exceeded 175 times, which was more than 2 times higher than that of the CCAM-ESG.

3. The spalling of asphalt film on aggregate surface was also a vital reason for CCAM freeze-thaw damage.

Microstructure

Experimental Method

In this study, the microstructure of the hardened CCAM was observed by using a scanning electron microscope, QUANTA 250, produced by FEI Company. This device was equipped with a cold field emission electron gun operating at 15kv.

The crushed pieces of the hardened CCAM were first soaked in an absolute ethyl alcohol solution to stop hydration, and then dried in a vacuum drying oven until a constant weight was reached. Finally, the surface of the sample was sputter coated with a thin layer of platinum/palladium (Pt/Pd) before the SEM observation.

Interior Structure of CCAM

Figure 4.28 shows the interior structure of the CCAM.

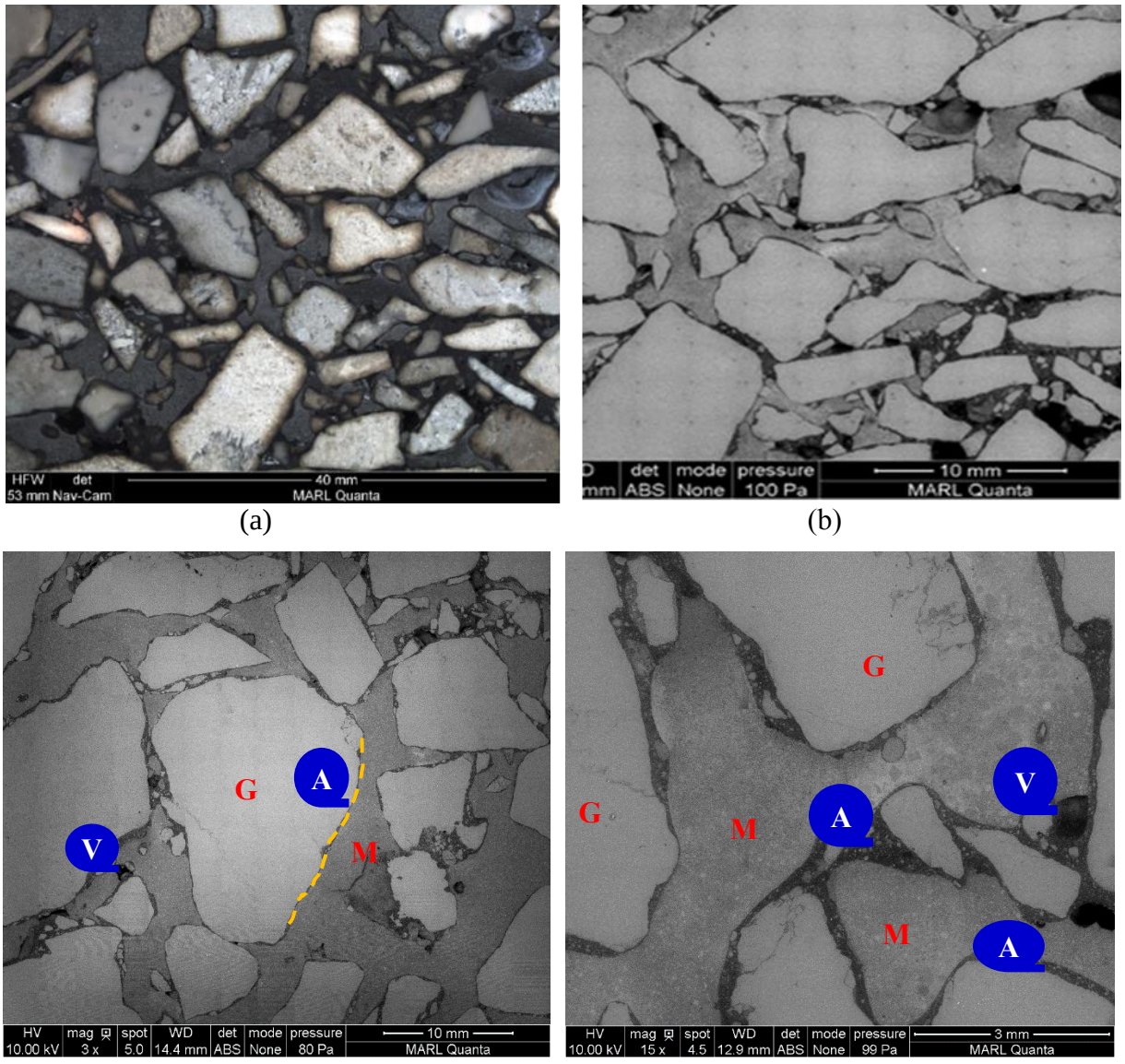

(a) (b)

(c) (d)

G: aggregate, A: asphalt mortar, M: hardened grout, V: air void

Figure 4.28. Interior structure of CCAM

Figure 4.28(a) and (b) show that the CCAM presented a denser appearance overall despite the existence of less porosity in certain partial areas. This density could be attributed to the porosity of the porous asphalt mixture that was effectively filled by the grouting material.

In addition, the coarse and fine aggregates were distributed uniformly in the CCAM, and the basic framework structure of the CCAM formed due to embedding between the different coarse aggregates. The ensuing stone-to-stone contact of aggregates with each other was beneficial to improving the rutting resistance capacity of the CCAM.

The CCAM is mainly composed of four parts: aggregates, asphalt mortar, hardened grouting material, and the unconnected pores, which are denoted by G, M, A and V, respectively in Figure 4.28. According to the mix ratio of porous asphalt mixture and its air-void percent in Chapter 3, the porosity of the porous asphalt mixture can be calculated approximately. The volume fraction of the aggregates and asphalt mortar accounted for about 75% of the total volume, while the volume fraction of the hardened grouting material and the unconnected pores accounted for 25% of the total volume.

According to the mix ratio of the porous asphalt mixture, particles of over 0.15 mm could be considered as aggregates, while the asphalt mortar was formulated by mixing the asphalt with the particles of less than 0.15 mm. In this case, it can be calculated that the volume fraction of the aggregate and the asphalt mortar accounted for about 67% and 7.4%, respectively, of the total volume as shown in Table 4.7. The volume fraction of the unconnected pores is discussed in the next section.

Table 4.7. Volume fraction of aggregate and asphalt mortar

Materials	Type (mm [in.])	Weight (%)	Weight (kg/m^3)	Density (kg/m^3)	Volume (%)
Aggregate	>0.15 mm [No. 100]	93.3	1790.4	2.67	67.0
Asphalt mortar	<0.15 mm [No. 100]	3.8	72.9	2.67	2.7
Asphalt	PG 76-28	2.9	55.9	1.20	4.7
Total		100	1919	/	74.4

Unfilled Air Void

Figure 4.29 shows a cross section of the CCAM, while Figure 4.30 depicts the partial enlargement of the unfilled air void.

Figure 4.29. Cross section of the CCAM

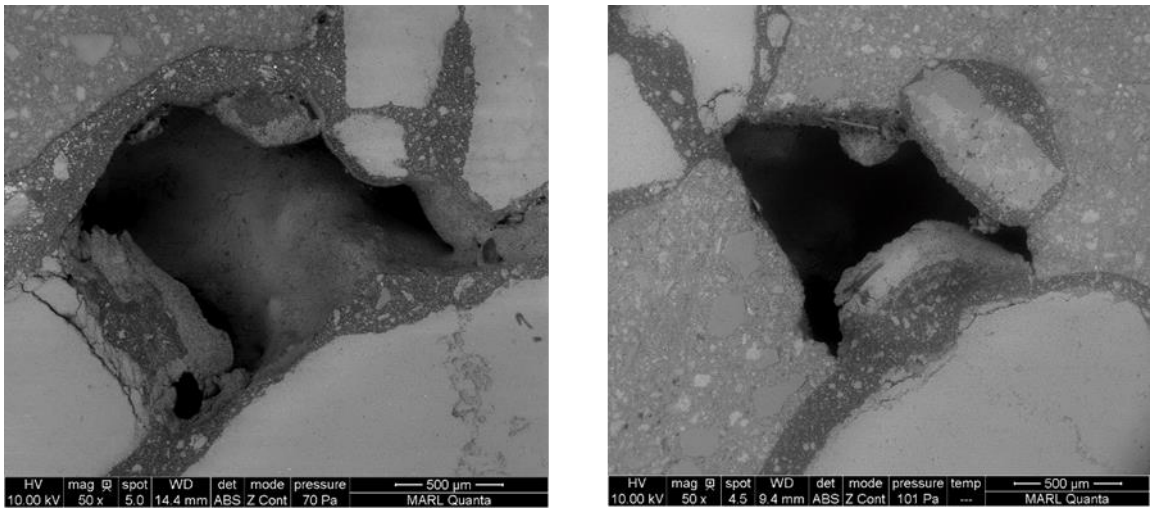

Figure 4.30. Unfilled air void of the CCAM

From Figure 4.29, it can be seen that some pores unfilled by grouting material are not distributed uniformly in the inner area of the CCAM, and the pores (which are about 5 mm) are irregularly shaped. Most of the pores distributed around the aggregates, or in the gaps between the aggregates, were not distributed within the inner section of the hardened grouting material. Meanwhile, the pore walls contained asphalt mortar, which indicated that the pore formation was accompanied by the formation of porous asphalt mixture with large porosity, but the porosity had not been introduced by the grouting material.

There are two possibilities behind the formation of pores in the CCAM: (1) poor workability of the grouting material or (2) the pores are unconnected and can't be filled effectively. In order to analyze the volume fraction and the reason for the formation of the unconnected pores, the connected porosity of the asphalt mixture was measured by immersing in water before grouting.

(It is assumed that pores which cannot be penetrated by water could be considered as unconnected pores.) The porosity of the unconnected pores could then be calculated by subtracting the porosity of the connected pores from the total porosity. The porosity of the CCAM could be confirmed by combining the experimental and calculating methods after grouting.

Finally, the reason for the formation of the pores could be summarized by comparing the porosity of the unconnected pores in the porous asphalt mixture with the porosity of the CCAM. When the porosity of the unconnected pores is closer to that of the CCAM, it can be deduced that the unconnected pores that cannot be filled fully could be considered as a dominant reason for the formation of the porosity. In other cases, when the porosity of the CCAM is significantly higher in comparison to that of the unconnected pores, the main reason for the formation of the pores in the CCAM could be the poor workability of the grouting material.

Immersion penetration is the special process for measuring the porosity of a porous asphalt mixture. The steps using this method were as follows:

1. The cylinder specimen was prepared according to the mix ratio and the preparation method for porous asphalt mixture introduced in Chapter 3.

2. The total volume of V0 and the total porosity VA were calculated.

3. The mass of dry sample in the air denoted as ma and the mass of sample under water denoted as mw were measured.

The mass difference was calculated by subtracting mw from ma, and the ratio of the mass difference to the density of water was the total volume denoted as VAM, including the volume of the asphalt mixture and the volume of the unconnected pores. The porosity of connected pores denoted as VAc was the ratio of the volume difference gained by subtracting VAM from V0 and the total volume of V0, and the porosity of the connected pores denoted as VAnc could be calculated by subtracting VAc from VA. The special calculating method is shown below:

$$V_{AM} = (m_a - m_w) \div \rho_w \quad (1)$$

$$V_{Ac} = 100 - 100 \times V_{AM} \div V_0 \quad (2)$$

$$V_{Anc} = V_A - V_{Ac} \quad (3)$$

Where, ma = mass of dry sample in air, g; mw = mass of sample under water, g; V0 = total volume of sample; VAM = volume of asphalt mixture without air voids; VA = total porosity of porous asphalt mixture; VAc = connected porosity of porous asphalt mixture; VAnc = non-connected porosity of porous asphalt mixture; and ρ w= density of water at 25°C, 0.9971 g/cm3.

Table 4.8 shows the results of connected and non-connected porosity of porous asphalt mixture.

Table 4.8. Connected and non-connected porosity of porous asphalt mixture

Sample	Size (mm)	Gyration number	V_0 (cm^3)	m_a (g)	m_w (g)	V_{AM} (cm^3)	V_A (%)	V_{Ac} (%)	V_{Anc} (%)
No. 1	φ133.7×100	50	1050	1989	1186	806	25.9	23.2	2.7
No. 2	φ134.0×100	50	1052	2024	1205	822	24.4	21.9	2.5
No. 3	φ133.9×100	50	1051	2021	1198	825	24.6	21.5	3.1
No. 4	φ127.8×100	100	1003	2032	1214	820	20.7	18.3	2.4

All of the specimens were prepared with the same mix and raw materials, the range of VA varied from 20.7 to 25.9% with various gyration numbers. As can be seen in Table 4.8, the value of VAnc varies slightly from 2.4 to 3.1% for various VA and their mean value is 2.7%.

The method of measuring and calculating the porosity of the CCAM after grouting could be summarized as: the total volume, total porosity, and mass of the specimen of porous asphalt mixture were measured before grouting, and are denoted as V0, VA, and ma, respectively. Next, the flowable grouting material was prepared by mixing with water, the bulk weight of which was measured and denoted as ρ G. The porous asphalt mixture was grouted by the grouting material, the extra grouting material was removed from the surface of the porous asphalt mixture, and the mass of the hardened specimen was measured and denoted as mc. Therefore, the mass of the grouting material denoted as mG could be calculated by subtracting ma from mc, meaning that the volume of grouting material could be calculated by dividing mG to ρ G, and the volume fraction of grouting material denoted as VG was the ratio of the volume of the grouting material to V0. Therefore, the porosity of the unconnected pores denoted as VAuf could be calculated by subtracting VG from VA.

The results of the unfilled air void of the CCAM are presented in Table 4.9.

Table 4.9. Unfilled air void of CCAM

No. of sample	Specimen size (mm)	m_a (g)	m_G (g)	V_G (%)	V_{Auf} (%)
1	Cylinder φ100×133.7	2030	449	21.2	3.6
2		2030	464	21.9	2.9
3		2030	482	22.7	2.1
4		2030	469	22.1	2.7
5		2030	471	22.2	2.6
6	Cylinder φ100×100	1510	370	23.3	1.5
7		1510	366	23.0	1.8
8		1510	362	22.8	2.0
9		1510	363	22.9	1.9
10		1510	357	22.5	2.3
11		1510	347	21.9	2.9

Note: ρ_G=2.02 g/cm^3, V_A=24.8%

From Table 4.9, it can be seen that the values of VAuf vary from 1.5 to 3.6%, which is close to VAnc. However, the variation range is significantly larger than that of VAnc. A possible reason is that the outside surface of the specimen has either more or less grout than is needed for the CCAM.

In order to avoid this problem, a plate specimen was prepared. All the surfaces of the specimen were cut to the depth of about 2 cm after hardening, the mass of the specimen was measured, and denoted as mc. The volume of the specimen denoted as V0 could be measured by the volume of the water that the specimen displaced after being immersed in water. The mass of the asphalt mixture denoted as mA could be calculated via V0 multiplied by the density of the porous asphalt mixture (1.919 g/cm3). The mass of the grouting material denoted as mG could be calculated by subtracting mc from mA. That is, the volume of the grouting material could be calculated by dividing mG to ρ G, as the volume fraction of grouting material denoted as VG was the ratio of the volume of the grouting material to V0. Therefore, the porosity of the unconnected pores denoted as VAuf could be calculated by subtracting VG from VA. The test results appear in Table 4.10.

Table 4.10. Unfilled air void of CCAM

Sample No.	Specimen size (mm)	m_a (g)	m_G (g)	V_G (%)	V_{Auf} (%)
1	70.72×60.05×104.97	1055.53	200.08	22.2	2.6
2	57.89×78.13×303.04	-	625.59	22.6	2.2

Note: ρ_G=2.02 g/cm^3, V_A=24.8%

Microstructure of Cement Mortar

The microstructure and hydration products of hardened grout are shown in Figure 4.31 and Figure 4.32, respectively.

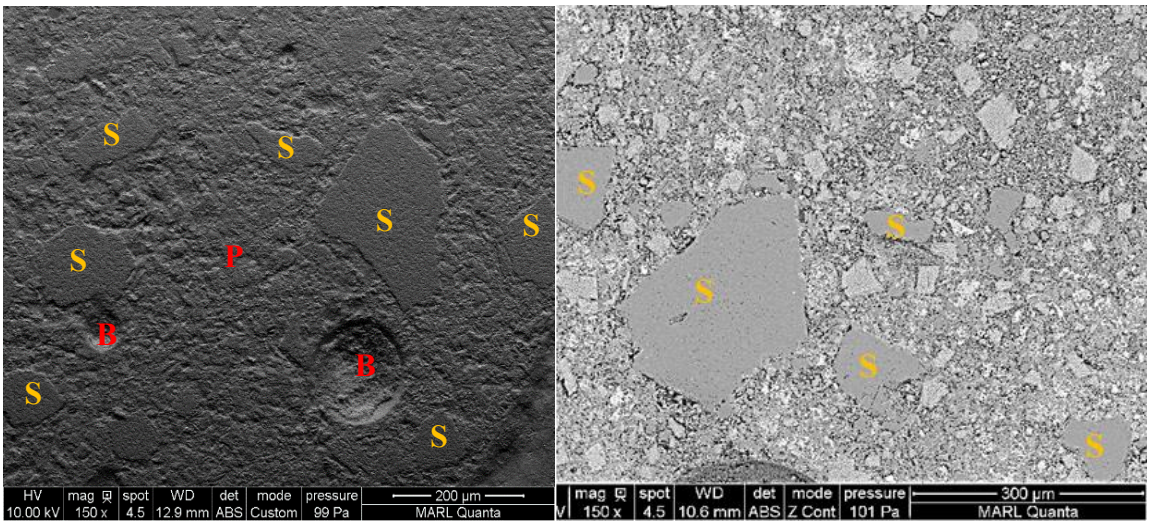

(a) (b)

S: silica sand, P: cement paste, B: air bubble

Figure 4.31. Microstructure of hardened grout

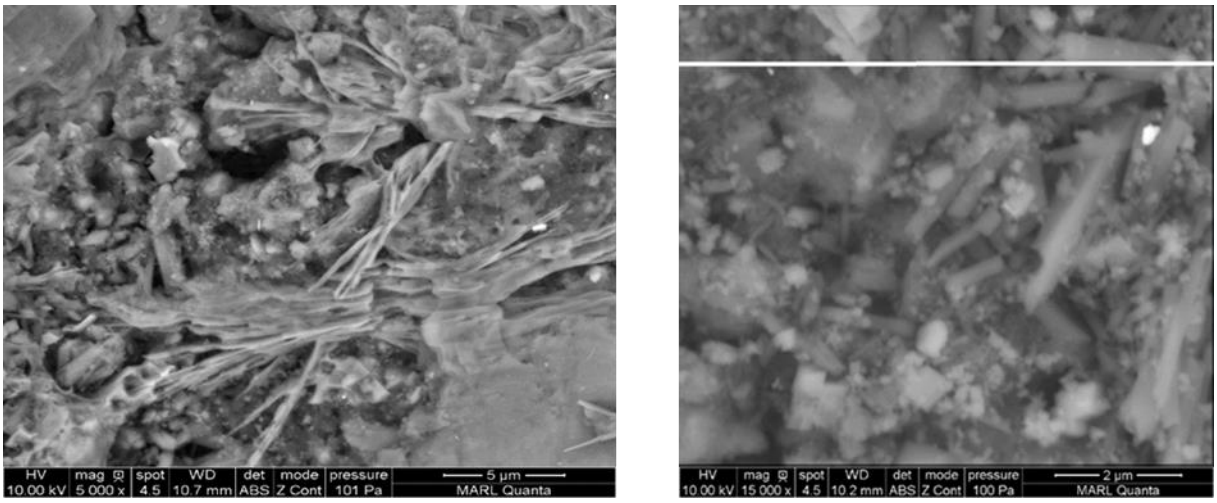

(a) (b)

Figure 4.32. Hydration products of hardened grout

In Figure 4.31, it can be seen that the hardened grout is very dense except for a small amount of air bubbles. A lot of fine silica sand in various sizes (no more than 0.2 mm) is distributed uniformly in the hardened cement paste.

In Figure 4.32(b), some sticks or columnar hydration products can be seen. Figure 4.33 indicates that characteristics of hydration products include high contents of aluminum, calcium, and sulfur, and low silicon content. Notably, in the upper right corner of Figure 4.32(b), the hydration products have characteristics of high aluminum and low sulfur content, while the lower left corner shows the opposite characteristics of high sulfur and low aluminum content. As described previously, the ESG grout used in this study was made with calcium sulphoaluminate cement.

When considering the morphology characteristics of hydration products, it can therefore be concluded that the major hydration products are hydrated calcium sulphoaluminate, consistent with high sulfur content.

The electron dispersive spectroscopy (EDS) spectra of hydration products in Figure 4.32(b) is shown in Figures 4.33 and 4.34.

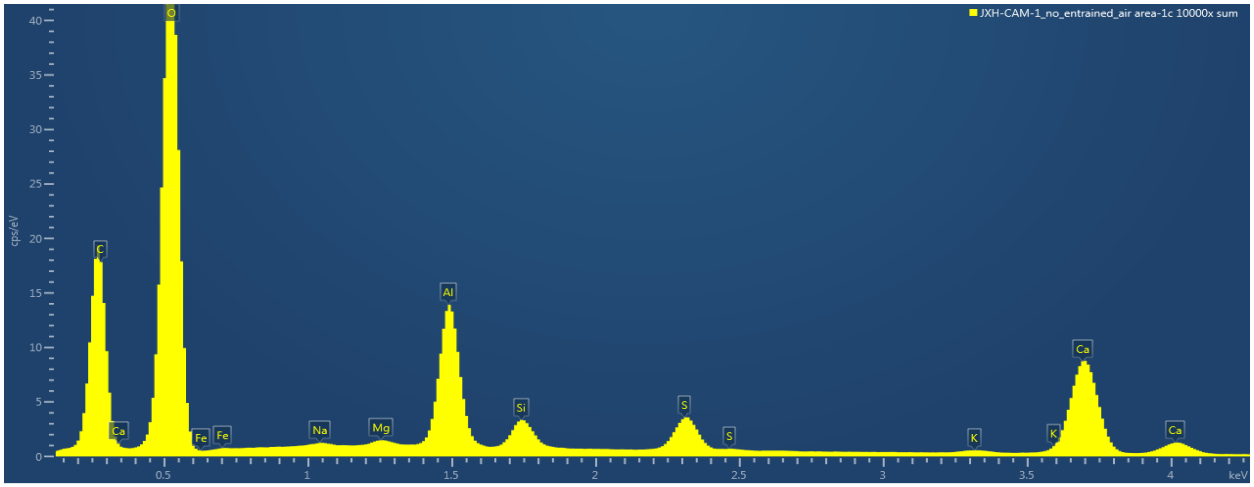

Figure 4.33. EDS spectra of hydration products

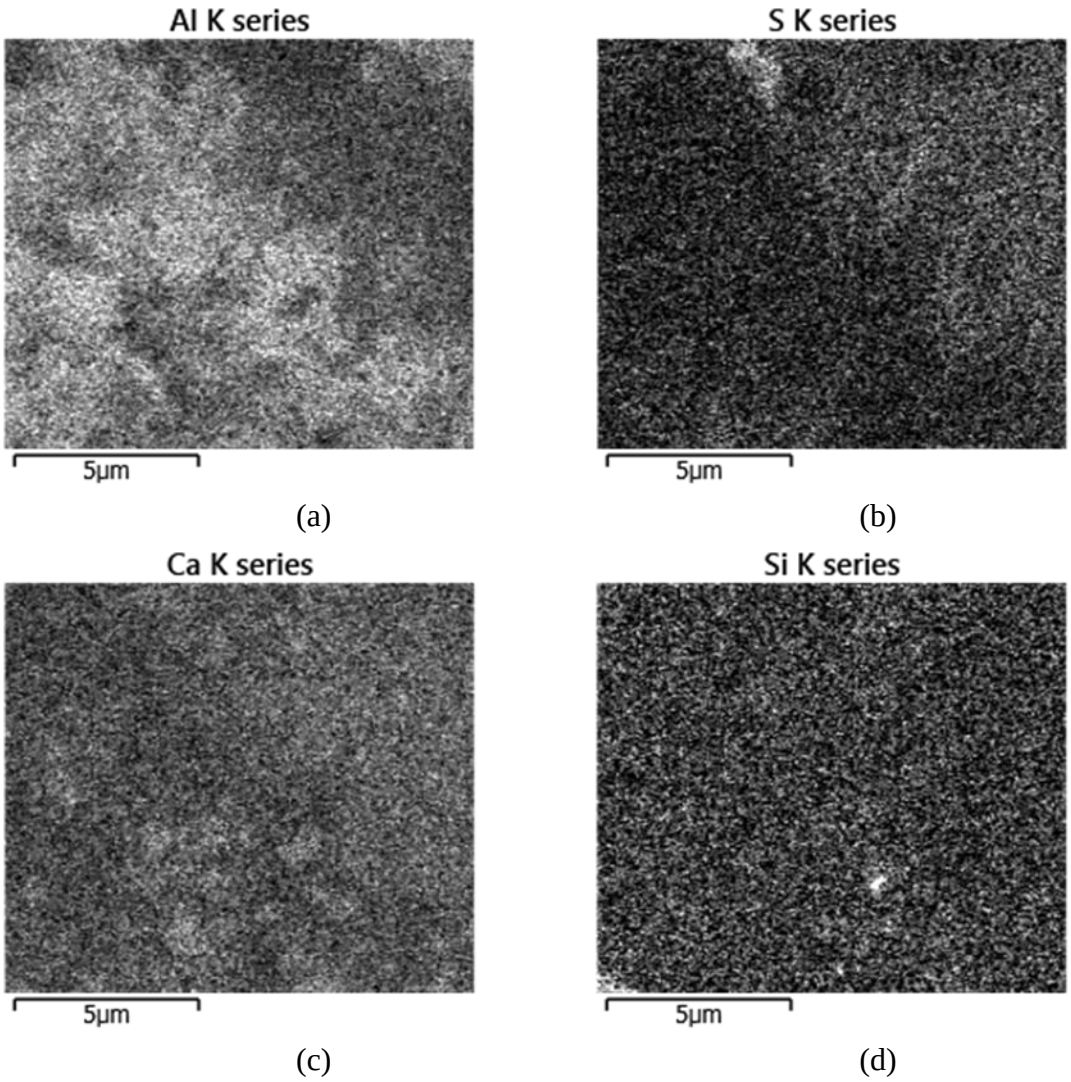

Figure 4.34. EDS spectra of hydration products

Microstructure of Asphalt Mortar

Microstructure of asphalt mortar is shown in Figures 4.35 through 4.37. From Figure 4.35, it can be seen that asphalt mortar is very dense at the three magnifications of 50×, 1500×, and 5000×. Figures 4.35 through 4.37 indicate that the thickness of asphalt mortar is approximately 30 μm.

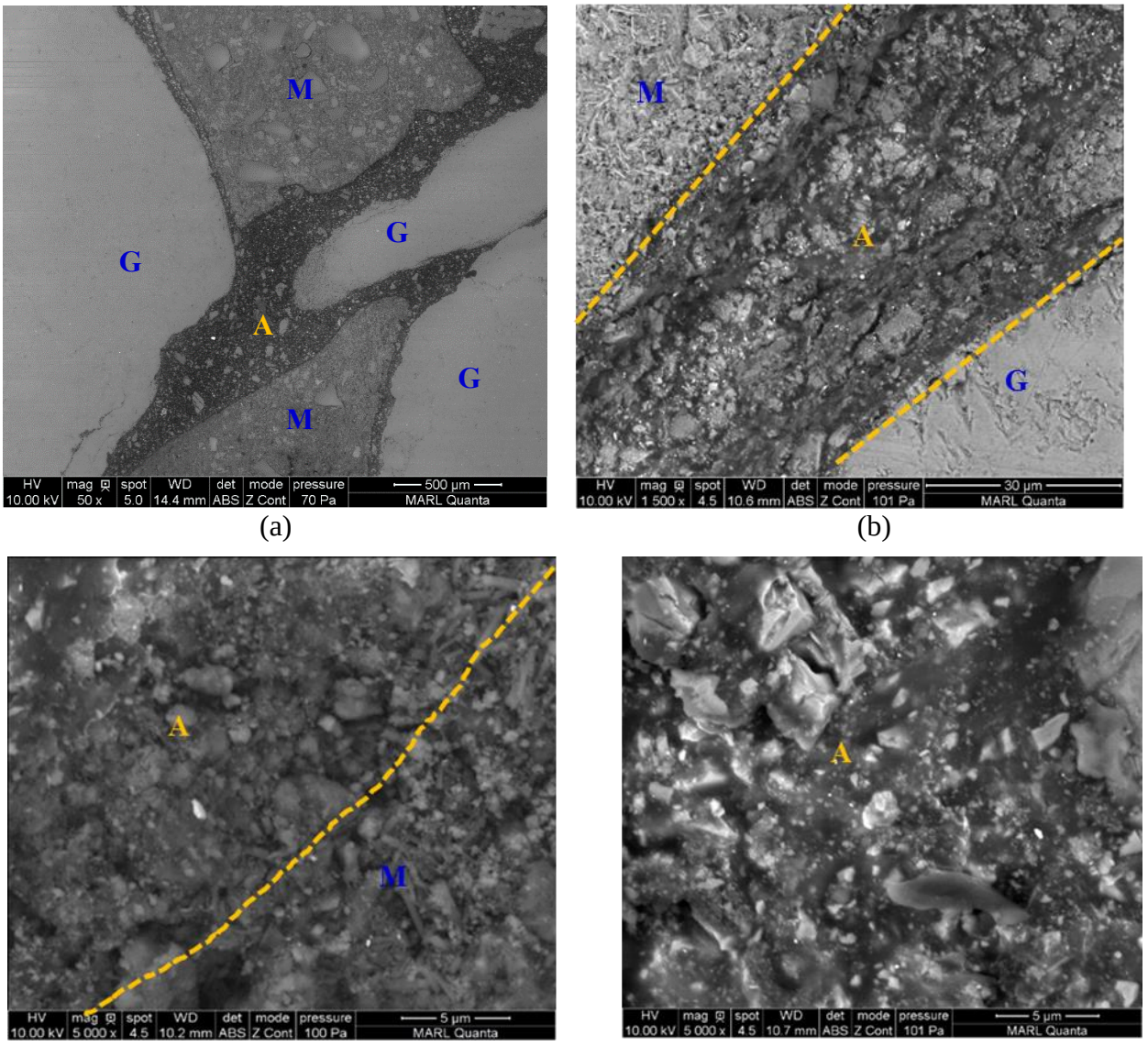

(a) (b)

(c) (d)

Figure 4.35. Microstructure of asphalt mortar

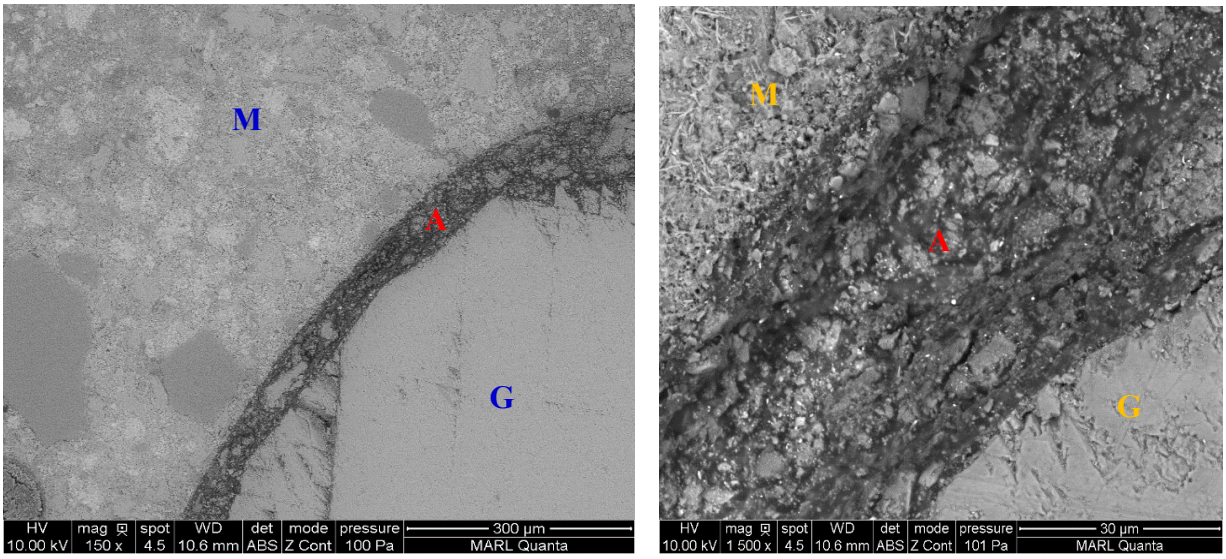

(a) (b)

Figure 4.36. Microstructure of asphalt mortar

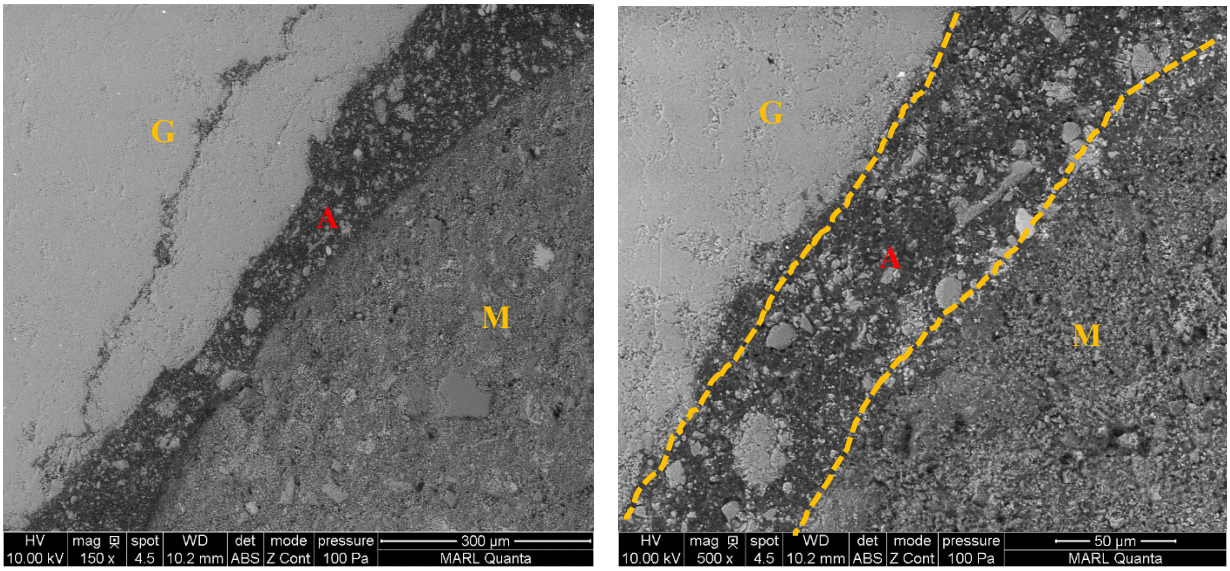

(a) (b)

Figure 4.37. Microstructure of asphalt mortar

Interfacial Transition Zone

The interfacial transition zone is a key component of composite, capable of exerting significant influence on the composite properties. The CCAM is a kind of organic-inorganic composite, formed by rolling or grouting the mixture composed of aggregates and two types of binder, including cement and asphalt. In comparison to asphalt concrete or cement concrete, the microstructure of the interfacial transition zone in the CCAM is much more complicated. Three kinds of interfacial material exist in the CCAM, including the interfacial zones between asphalt

and aggregates in the porous asphalt mixture, between cement and asphalt after grouting of the cement paste, and between the cement paste and fine aggregates.

Figures 4.35 through 4.37 show that there is little obvious evidence of an interfacial transition zone between asphalt or aggregates and cement. Similarly, the excellent interfacial bonding presented between the fine aggregates and the cement paste in the grouting material, as shown in Figure 4.31, is significantly different from the interfacial transition zone in common concrete with a width of about 20–40 μm, and a large amount of CH as well as high porosity. The results suggested excellent interfacial bonding took place, including the interfacial zone between asphalt and aggregates, and the interfacial zone between cement paste and asphalt or aggregates.

CONCLUSIONS AND RECOMMENDATIONS

A hybrid, made with asphalt (flexible) pervious concrete filled with Portland cement (rigid) mortar, called a casting cement asphalt mixture (CCAM), was developed. Experiments were conducted on CCAMs made with Iowa concrete materials in various proportions to achieve optimal porosity of asphalt pervious concrete and optimal flowability of mortar for CCAMs. The basic engineering properties of these CCAMs, such as strength, shrinkage, and freeze-thaw durability, were then evaluated. The following conclusions were drawn:

1. A CCAM can be successfully produced with a pervious concrete of 25% porosity and a very highly flowable, rapid set cement grout. Although the grout used was highly flowable, around 2.4%, voids in the porous asphalt concrete still could not be filled. Overuse of superplasticizer for flowability could lead to segregation and water bleeding, which exerts an adverse effect on the formation of the microstructure and the compressive strength.

2. The early-strength grout (ESG) produced from calcium sulphoaluminate cement developed compressive strength over 18 MPa (2600 psi) in less than 12 hours. This permits a CCAM pavement to be open to traffic at a much earlier time than a conventional Portland cement concrete roadway. The strength of the high-strength grout (HSG) produced from Portland cement can be further enhanced by using a combination of fly ash and silica fume.

3. The contributive efficiency of grouting material to the strength of CCAM increased with curing time. At the age of 28 days, grout was responsible for 40% while the asphalt matrix is responsible for 60% of the overall compressive strength of the CCAM.

4. The CCAM showed higher resilient modulus and better rutting performance than traditional asphalt mixtures. Asphalt concrete failed at 9 mm rut after being subjected to 10,000 wheel track cycles during a wheel track rutting test, while the CCAM showed less than a 1 mm rut during the test. Although CCAM-HSG and CCAM-ESG showed similar compressive modulus, the CCAM-HSG exhibited lower rutting depth than the CCAM-ESG, which indicated that selection of a high modulus grouting material can make a CCAM less susceptible to rutting.

5. The microstructure analysis showed that there were excellent bonds between asphalt and aggregate as well as between asphalt-coated aggregate and cement. The CCAM also showed acceptable anti-moisture capability based on IDT ratio analysis.

6. Although the CCAM has attracted a great deal of attention in Europe and Asia, most applications have been in warm climate regions. Few or no applications of CCAMs have been conducted in the US, particularly in cold climate regions. Further investigation needs to be done on the CCAM freeze-thaw durability before this new material is applied to Iowa pavements.

7. As CCAMs are neither asphalt nor Portland cement concrete, a major project challenge was to find appropriate test methods for evaluating key properties of the CCAM, especially the method for testing freeze-thaw durability. In this study, ASTM C666-B was used for testing CCAM freeze-thaw durability, which might not be most appropriate. Development of new test methods may be necessary.

8. The grouting materials used contained a large portion of fine particles. Having proper air entrainment and a stable air system in the grout pastes was also found very challenging. Further studies are necessary on the freeze-thaw durability of CCAMs to overcome these challenges and significantly extend the applications of this new technology.

REFERENCES

AASHTO. 2005. *Standard Specification for Air-Entraining Admixtures for Concrete*. M 154. American Association of State Highway and Transportation Officials, Washington DC.

AASHTO. 2007. *Standard Method of Test for Determining the Creep Compliance and Strength of Hot Mix Asphalt Using the Indirect Tensile Test Device*. T 322. American Association of State Highway and Transportation Officials, Washington DC.

AASHTO. 2010. *Standard Method of Test for Compressive Strength of Bituminous Mixtures*. T 167. American Association of State Highway and Transportation Officials, Washington DC.

AASHTO. 2011. *Resistance of Compacted Bituminous Mixture to Moisture-Induced Damage for Superpave*. T 283. American Association of State Highway and Transportation Officials, Washington DC.

Afonso, M., M. D. Almeida, L. Oliveria, J. C. Gomes, and S. E. Zoorob. 2016. Development of a Semi-Flexible Heavy Duty Pavement Surfacing Incorporating Recycled and Waste Aggregates – Preliminary Study. *Construction and Building Materials*, Vol. 102, No. 1, pp. 155–161.

American Concrete Institute Committee 237. 2007. *Self-Consolidating Concrete*. 237R-07. American Concrete Institute, Farmington Hills, MI.

ASTM. 2000. *Standard Specification for Air-Entraining Admixtures for Concrete*. C260, ASTM International, West Conshohocken, PA.

ASTM. 2002. *Standard Test Methods for Sands Equivalent Value of Soils and Fine Aggregate*. D2419. ASTM International, West Conshohocken, PA.

ASTM. 2005. *Standard Specification for Portland Cement*. C150. ASTM International, West Conshohocken, PA.

ASTM. 2010. *Standard Test Method for Flat Particles, Elongated Particles, or Flat and Elongated Particles in Coarse Aggregate*. D4791. ASTM International, West Conshohocken, PA.

ASTM. 2011. *Standard Test Method for Theoretical Maximum Specific Gravity and Density of Bituminous Paving Mixtures*. D2041. ASTM International, West Conshohocken, PA.

ASTM. 2011. *Standard Test Method for Percent Air Voids in Compacted Asphalt Mixtures*. D3203. ASTM International, West Conshohocken, PA.

ASTM. 2011. *Standard Test Method for Maximum Specific Gravity and Density of Asphalt Mixtures Using Automatic Vacuum Sealing Method*. D6857. ASTM International, West Conshohocken, PA.

ASTM. 2011. *Standard Test Method for Determination of Draindown Characteristics in Uncompacted Asphalt Mixtures*. D6390. ASTM International, West Conshohocken, PA.

ASTM. 2013. *Standard Test Method for Resistance to Degradation of Small-Size Coarse Aggregate by Abrasion and Impact in the Los Angles Machine*. C131. ASTM International, West Conshohocken, PA.

ASTM. 2013. *Standard Test Method for Determining the Percentage of Fractured Particles in Coarse Aggregate*. D5821. ASTM International, West Conshohocken, PA.

ASTM. 2017. *Standard Test Methods for Uncompacted Void Content of Fine Aggregate*. C1252. ASTM International, West Conshohocken, PA.

Ballestero, T., J. Houle, and T. Puls. 2014. *UNHSC Design Specifications for Porous Asphalt Pavement and Infiltration Beds*. University of New Hampshire Stormwater Center, Durham, NH. https://www.unh.edu/unhsc/sites/unh.edu.unhsc/files/UNHSC%20PA%20Spec%20update-%20FEB-2014.pdf

Cai, J., J. Pei, Q. Luo, J. Zhang, R. Li, and X. Chen. 2017. Comprehensive Service Properties Evaluation of Composite Grouting Materials with High-Performance Cement Paste for Semi-Flexible Pavement. *Construction and Building Materials*, Vol. 153, pp. 544–556.

Deng, C., C. Huang, and J. Hong. 2016. Study of Super-Early-Strength Semi-Flexible Pavement Used in Municipal Road. *Central South Highway Engineering*, No. 1, pp. 116–119.

Ding, Q., Z. Sun, F. Shen, and S. Huang. 2011. The Performance Analysis of Semi-flexible Pavement by the Volume Parameter of Matrix Asphalt Mixture. *Advanced Materials Research*, Vols. 168-170, pp. 351–356.

Fang, B., T. Xu, and S. Shi. 2016. Laboratory Study on Cement Paste Formulation and Its Strength Mechanism for Semi-Flexible Pavement. *Journal of Testing and Evaluation*, Vol. 44, No. 2, pp. 907–913.

Hao, P., L. Cheng, and L. Lin. 2003. Pavement Performance of Semi-Flexible Pavement in Laboratory. *Journal of Xi'an Highway University*, No. 2, pp. 1–6.

Hou, S., T. Xu, and K. Huang. 2016. Investigation into Engineering Properties and Strength Mechanism of Grouted Macadam Composite Materials. *International Journal of Pavement Engineering*, Vol.17, No. 10, pp. 878–886.

Koting, S., M. R. Karim, and H. Mahmud. 2007. The Properties of Bituminous Mixtures for Semi-Flexible Pavement. Paper presented at the Seventh International Conference of Eastern Asia Society for Transportation Studies, September, Dalian, China.

Mayer, J. and M. Thau. 2001. Jointless Pavements for Heavy-Duty Airport Application: The Semi-Flexible Approach. Paper presented at Advancing Airfield Pavements: 27th International Air Transportation Conference, August 5–8, Chicago, IL. https://ascelibrary.org/doi/pdf/10.1061/40579%28271%297.

Merrill, D., A. V. Dommelen, and L. Gáspár. 2006. A Review of Practical Experience throughout Europe on Deterioration in Fully-Flexible and Semi-Rigid Long Life Pavements. *International Journal of Pavement Engineering*, Vol. 7, No. 2, pp. 101–109.

Pei, J., J. Cai, D. Zou, J. Zhang, R. Li, X. Chen, and L .Jin. 2016. Design and Performance Validation of High-Performance Cement Paste as a Grouting Material for Semi-Flexible Pavement. *Construction and Building Materials*, Vol. 126, pp. 206–217.

Research Institute of Highway. 2011. *Standard Test Methods of Bitumen and Bituminous Mixtures for Highway Engineering*. JTG E20-2011. Research Institute of Highway, Ministry of Transport, Beijing, China.

Setyawan, A. 2006. Development of Semi-flexible Heavy-duty Pavements. PhD thesis. School of Civil Engineering, University of Leeds, Leeds, UK.

Setyawan, A. 2013. Assessing the Compressive Strength Properties of Semi-Flexible Pavements. *Procedia Engineering*, Vol. 54, pp. 863–874.

Wei, Y., M. A. Biao, and S. I. Wei. 2012. Influencing Factors of Compression Strength of Asphalt Mixture in Cold Region. *Journal of Highway and Transportation Research and Development*, Vol. 29, No. 4, pp. 19–22.

Wu, G., Y. Wang, and R. Wang. 2010. A Study of the Strength Mechanism of Semi-flexible Composite Pavement Material and a Modified Method for the Determination of Its Compressive Resilient Modulus. Paper presented at the Tenth International Conference of Chinese Transportation Professionals (ICCTP), August 4–8, Beijing, China.

Yang, B. and X. Weng. 2015. The Influence on the Durability of Semi-Flexible Airport Pavement Materials to Cyclic Wheel Load Test. *Construction and Building Materials*, Vol. 98, pp. 171–175.

Zhang, J., J. Cai, J. Pei, R. Li, and X. Chen. 2016. Formulation and Performance Comparison of Grouting Materials for Semi-Flexible Pavement. *Construction and Building Materials*, Vol. 115, pp. 582–592.

THE INSTITUTE FOR TRANSPORTATION IS THE FOCAL POINT FOR TRANSPORTATION AT IOWA STATE UNIVERSITY.

InTrans centers and programs perform transportation research and provide technology transfer services for government agencies and private companies;

InTrans manages its own education program for transportation students and provides K-12 resources; and

InTrans conducts local, regional, and national transportation services and continuing education programs.

IOWA STATE UNIVERSITY

Visit www.InTrans.iastate.edu for color pdfs of this and other research reports.